Moderate-grade germinal matrix haemorrhage activates cell division in the neonatal mouse subventricular zone.

William J Dawes[1]*, Xinyu Zhang[1], Stephen P.J. Fancy[2], David Rowitch[2] and Silvia Marino[1]*

[1] Blizard Institute, Barts and The London School of Medicine and Dentistry, Queen Mary University of London, 4 Newark Street, London E1 2AT, UK

[2] Departments of Pediatrics and Neurosurgery, Eli and Edythe Broad Institute for Stem Cell Research and Regeneration Medicine and Howard Hughes Medical Institute, University of California San Francisco, 513 Parnassus Avenue, San Francisco, CA, 94143, USA

* Corresponding authors

William J Dawes and Silvia Marino

Blizard Institute, 4 Newark Street, London E1 2AT

Tel +44 207 882 2585,

Fax +44 207 882 2180,

Email: s.marino@qmul.ac.uk

Running title: Neural stem cells and neonatal brain haemorrhage

Abstract

Precise temporal and spatial control of the neural stem progenitor cells within the subventricular zone germinal matrix of the brain is important for normal development in the third trimester and early postnatal period. High metabolic demands of proliferating germinal matrix precursors, coupled with the flimsy structure of the germinal matrix cerebral vasculature, are thought to account for high rates of haemorrhage in extremely- and very-low birth weight preterm infants. Germinal matrix haemorrhage can commonly extend to intraventricular haemorrhage. Because neural stem progenitor cells are sensitive to micro-environmental cues from the ventricular, intermediate and basal domains within the germinal matrix, haemorrhage has been postulated to impact neurological outcome through aberration of normal neural stem/progenitor cells behaviour

We have developed an animal model of neonatal germinal matrix haemorrhage using stereotactic injection of autologous blood into the mouse neonatal germinal matrix. Pathological analysis at 4 days post injury shows high rates of intraventricular extension and ventricular dilatation but low rates of parenchymal disruption outside the germinal zone, recapitulating key features of human “Papile grade III” IVH. At 4 days post injury we observed proliferation in the wall of the lateral ventricle with significantly increased numbers of transient amplifying cells within the subventricular zone and corpus callosum. Analysis at 21 days post injury revealed that cortical development was also affected with increased neuronal and concomitant reduced oligodendroglial differentiation.

At the molecular level, we show down regulation of the expression of the transmembrane receptor Notch2 in $CD133^{+ve}$ cells of the SVZ, raising the possibility that the burst of precocious proliferation seen in our experimental mouse model and the skewed differentiation could be mediated by down regulation of the Notch pathway within the proximal / ventricular domain. These findings raise the possibility that Notch regulation plays a critical role in mediating the response of the neonatal SVZ to ischaemic and haemorrhagic insults.

Keywords

Neural stem/progenitor cells, postnatal gliogenesis, postnatal neurogenesis, germinal matrix haemorrhage, mouse models

Introduction

Delayed primigravida (first pregnancy) and the use of in vitro fertilisation have contributed to an increase in the incidence of premature birth in all developed countries [1,2] and despite advances in perinatal care, haemorrhage within the germinal matrix (GM) remains a commonly recognised complication seen in up to 45% of extremely premature babies weighing 500-750g [3]. The cause of brain injury associated with premature birth is complex and multifactorial with ischaemia [4] and inflammation [5] playing key roles. In addition to this outcome has been shown to correlate with the severity of haemorrhage with extension into the ventricle and loss of brain parenchyma secondary to porencephalic cyst formation being associated with significant neurodevelopmental disabilities [6-8]. The prevention of premature birth and reducing the incidence of haemorrhage remain key research goals. However, the need for new modalities of treatment to limit neurodisability in this vulnerable patient group is clearly evident.

In order for normal brain development to take place, the behaviour of the neural stem/progenitor cells (NSPC) is tightly regulated in both a temporal and spatial fashion. This occurs through the balance of the cell intrinsic mechanisms and micro-environmental factors [9,10]. The microenvironment within the GM in which the NSC reside can be conceptualised as consisting of three domains [10]; the proximal / ventricular domain which responds to signalling within the CSF [11] and from interaction with the ependymal cells [12], the intermediate zone in which the NSC responds to cues arising from the intermediate progenitor cells [13,14] and neurotransmitters released within the SVZ [15] and the distal / basal domain which is under the influence of cues from the circulation and endothelial cells [16]. Plausible mechanisms can be envisaged through which any and all of these micro-environmental domains could be affected due to GMH.

Whilst GABAergic interneurons are known to arise from the SVZ in the final trimester [17-19], lineage tracing experiments have highlighted the critical role that the GM plays in the production of astrocytic and oligodendrocytic precursors [20] with the majority of oligodendrocytes developing during late embryogenesis and early postnatal life [21]. This surge in progenitor formation coincides with the peak incidence of GMH (23-28 weeks) and given the critical role that the oligodendrocyte

lineage is likely to play in the encephalopathy of prematurity (EP) [22] we hypothesised that GMH might be responsible for a primary stem cell disorder in an otherwise developmentally normal brain (i.e. no underlying genetic / pathological abnormality) making it an appealing target for therapeutic intervention.

GMH is recognised to cause both destructive and developmental impacts on the developing brain of the premature neonate [23]. To date, published models of IVH have focused on modelling severe haemorrhage with large parenchymal defects seen [24-27]. This approach is likely to mask the more subtle developmental impact of IVH on the NSPC within the SVZ; as such we endeavoured to produce a model with minimal cortical disruption to uncover this subtle mechanism.

Combining stereotactic injection of autologous blood at P0 [28] with a thymidine labelling strategy at P1 [29], we show that GMH caused an activation of proliferation in the wall of the lateral ventricle, which eventually resulted in an altered cellular composition of the cortex with an increased number of neuronal elements and concomitant depletion of oligodendrocytes. Expression analysis of the CD133/Prominin-positive cell fraction (a transmembrane glycoprotein expressed by NSC and ependymal cells within the lateral ventricle during early postnatal development [30], demonstrated down-regulation of the expression of Notch2, a well-known regulator of NSPC function in the proximal / ventricular domain [9,31], in these cells following GMH.

Material and Methods

Animals

All procedures had Home Office approval (Animals Scientific Procedures Act 1986, PPL 70/7275). C57BL/6 mice were used throughout. Cages were checked daily and intracranial autologous blood injections were undertaken on the afternoon of the first day of life.

Stereotactic intracranial injection of autologous blood

To facilitate accurate and reproducible restraint of the P0 pup, modifications were made to a Narishige stereotactic frame based on the work of Merkle et al [28] (Figure 1A&B). P0 pups were anaesthetised on ice for 3 minutes and 30 seconds prior to being fixed into the frame and autologous blood, collected from the tail tip

(Microvette™ CB300 VWR) was injected via a customized 1cm 30-gauge needle; 1mm posterior & 1.5mm superior to the posterior border of the left eye with a forward angulation of 24 degrees and a depth of 2mm (Figure S1). In the Sham group all experimental conditions were equivalent with the exception that the mice underwent needle injection only without blood injection.

EdU administration

Intraperitoneal injections of EdU (12.5mg/kg) (Life technologies™) were given on day 1 of life, according to published protocols [29].

Immunohistochemistry and histology

Mice were transcardially perfused under terminal anaesthesia with 0.9% saline followed by 4% paraformaldehyde. (PFA). Brains were dissected and post-fixed for 2 hours in 4% PFA at 4°C. Tissue was cryoprotected with 30% sucrose overnight, mounted in O.C.T. (VWR™) medium and sectioned at 10µm on a cryostat (Leica™).

For EdU staining samples were blocked with 3% BSA (Sigma™)/ Phosphate-Buffered Saline (PBS)/0.1% Triton X100 and incubated for 30 minutes with proprietary Click-iT® solutions (Life technologies™). For immunofluorescent double staining the following antibodies were used: Rabbit anti-GFAP 1:400 (Dako™): Rabbit anti-NG2 1:200 (Millipore™): Guinea Pig anti-Dcx 1:2000 (MerckMillipore™): Mouse anti-NeuN 1:100 (Millipore™): Mouse anti-MASH1 1:200 (BD Biosciences™): Rabbit anti-Iba1 1:100 (Wako™): Mouse anti-Olig2 1:500 (Charles-Stiles Lab). All incubations with primary antibody were undertaken overnight. After washing with PBS, sections were incubated with appropriate Alexa Fluor® secondary antibodies diluted 1:500 (Invitrogen™) for 2 h at room temperature, washed in PBS and mounted in Fluoromount™ (Sigma Aldrich™) or Vectashield® with DAPI (Vector Laboratories™).

Volumetric analysis using the Cavalieri probe

To quantify ventricular volume we adopted a stereological approach using the Cavalieri estimator probe within Stereoinvestigator MBF Bioscience™. In the Coronal plane volumetric analysis was undertaken between the induseum griseum (anterior zero section) and the appearance of the hippocampus in continuity across the midline (posterior zero section) (Figure S2) with every tenth section analysed. In the sagittal plane volume acquisition was undertaken from the sagittal zero section

(Figure S3) (defined as the first appearance of the striatum within the rostral migratory stream) and two further sections at 150 μ m & 300 μ m medial to the sagittal zero.

Image acquisition and analysis

All images were acquired using the Zeiss™ 710LSM Confocal Microscope at 40x Oil immersion objective lens and analysed using either tile scanning and Image J™ or the Optical Fractionator probe of Stereoinvestigator (MBF Bioscience™). For analysis of the subventricular zone, 3 coronal specimens per sample were analysed: Zero slide (Z) Z+150 μm & Z+300 μm, with all cells counted within the lateral and superior wall of the ventricle within the immediate hypercellular periventricular region, any staining which was not clearly nuclear was not counted. Within the corpus callosum a 300 pixel wide counting frame was taken through the corpus callosum positioned anterior to a perpendicular line taken from the anterior border of the hippocampus through the cortex (Figure 3). 3 samples per specimen were analysed: Sagittal - Z, Z-150 μm & Z-300 μm. Within the neocortex quantification was undertaken on 3 sagittally orientated samples with all neocortex included anterior to a perpendicular line taken from the anterior border of the hippocampus (Figure 4A).

Behavioural analysis

Daily behavioural analysis between P2 and P21 was undertaken. Reflex development was assessed using grip strength, negative geotaxis, cliff aversion and surface righting (Figure S4). Neuromotor development was assessed for three minutes in a Perspex open field chamber 50cm by 50cm: the number of head, shoulder pelvis lifts, head pointing and sniffing, sitting, rearing and falls were recorded using key presses, whilst distance travelled and speed was recorded using proprietary Anymaze software.

Extraction amplification and analysis of RNA from $CD133^{+ve}$ cell fraction

Following removal of the cerebellum and olfactory bulbs the left hemisphere was mechanically and enzymatically homogenised using the Miltenyi Biotec™ Neural Tissue dissociation kit®. Due to the small sample size wash volumes were reduced and all collections were made into 1ml Eppendorf tubes. Homogenised samples were filtered through 30 μm pre-separation filters (Miltenyi Biotec™), incubated with CD133 microbeads (Miltenyi Biotec™) and passed through the MACS® separation columns (Miltenyi Biotec™).

RNA extraction was undertaken using the RNeasy® Micro kit (Qiagen™). 20ng of extracted RNA from each sample was amplified using the QuantiTect® Whole Transcriptome kit (Qiagen™). The PCR array was then carried out on each amplified RNA product using the Mouse Stem Cell RT² Profiler™ (Qiagen™) to identify the potential targeted genes related to stem cell biology.

ISH analysis

The Hes 5 probe was kindly donated by Kriegstein lab (previously published in Muzio et al 2005[32]) and the in situ hybridization was carried out according to standard protocols[33].

Statistical analysis

Statistical analysis was undertaken using GraphPad Prism, t-test and one-way ANOVA in conjunction with Tukey's test for multiple comparisons were applied for comparisons between two datasets or multiple datasets respectively. A linear growth model was used to compare behavioural parameters.

Results

Establishment of a mouse model of GMH by stereotactic injection of autologous blood into the neonatal mouse subventricular zone.

In our hands using a published freehand injection of 15ul of autologous blood with a 26 gauge needle into the newborn mouse pup [26] caused significant morbidity and mortality and was associated with high levels of subdural extension of blood, significant damage to the surrounding cortex and marked variability in the injection site.

Stereotactic injection in newborn mouse pups using conventional equipment is limited due to the lack of restraints, as such modifications were made to a Narishige stereotactic frame based on the work of Merkle et al [28] (Figure 1A). The custom-made clay mould (Figure 1A inset), in combination with nose and body taping (Figure 1B) facilitated accurate and reproducible restraint.

Tissue dye injection into euthanized newborn (P0) mouse pups followed by histopathological examination of coronal brain samples was used to define injection coordinates and trajectory (Figure S1). The site of blood bolus, its vicinity to the anterior SVZ, the degree of damage to the surrounding parenchyma and the rate of intraventricular spread in comparison to subdural extension were analysed. Optimal injection coordinates were found to be; 1mm posterior and 1.5mm superior to the posterior border of the eye with a forward angulation of 24 degrees, at a depth of 2mm (Figure 1C and Figure S1). The longer trajectory used in the forward angulated approach was found to reduce bleed back along the needle tract with an increased volume of the SVZ seen to be affected by the blood bolus, it also facilitated injecting the anterior SVZ without the risk of damaging the eye. The needle used for injection was a custom-made Hamilton™ 30 gauge 1cm needle, lower gauge needles were associated with increased mortality and caused unacceptably high levels of tissue damage, higher gauge needles were liable to bend or slip, reducing the reproducibility of the injection site. We injected 5ul of whole blood, an amount that is easily and atraumatically extracted from the tail tip and does not significantly impact on the circulating volume, it also limits the adverse impact of bolus size on tissue distortion and intracranial pressure.

Histological analysis was carried out on coronally sectioned brains at day 1(P1) following stereotactic blood injection on the day of birth (P0) and it showed the haematoma to be consistently located within the SVZ with variable intraventricular spreading (Figure 1D). Minimal damage to the surrounding cortex was noted and overall mortality was low at day 4 with no late mortality seen. At day 4 (P4) an incipient haematoma cavity was noted within the SVZ with frequent cells of macrophagic lineage scavenging blood products within the SVZ, in keeping with siderophages (macrophages laden with iron) (Figure 1E).

We show that modification to the Narishige stereotactic frame as described above facilitates accurate and reproducible lesioning within the SVZ of the newborn mouse pup and could represent a useful tool to study the effect of GMH on the SVZ NSPC and on early cortical development.

GMH causes ventriculomegaly at P4, which persists up to P21

Histological examination of Nissl stained samples demonstrated significant ventriculomegaly in the blood-injected samples in comparison with the control samples. To quantify ventricular volume we adopted a stereological approach using the Cavalieri estimator probe within Stereoinvestigator MBF Bioscience™. Due to the potential distortion of the parenchyma in the rostrocaudal plane secondary to GMH, volumetric analysis was undertaken between fixed anterior and posterior points to ensure reproducibility. Using the indusium griseum / first appearance of the corpus callosum in continuity as the most anterior slide and the appearance of the hippocampus in continuity across the midline as the posterior slide (Figure S2A-D) an equal number of sections was generated for analysis (Control (n=8) 73.63 sections ± 3.8, Sham (n=5) 73.4 ± 2.4 GMH (n=7) 77 sections ± 4.8, p=0.78 ANOVA) (Figure S2E).

Quantitative assessment of volume in the coronal plane between the induseum griseum and the first appearance of the hippocampus in continuity revealed that blood injection causes significant ventriculomegaly at P4 (Control (n=7) 0.054mm^3 ± 0.007, Sham (n=4) 0.053mm^3 ± 0.003, GMH (n=5) 0.078mm^3 ± 0.005, p=0.02 ANOVA) (Figure 1F) and this was shown to persist up to P21 (Control (n=5) 0.003 mm^3 ± 0.0004 GMH (n=4) 0.015 mm^3 ± 0.005 p=0.03 t-test) (Figure 1G-H). Ventriculomegaly was not seen in the sham mice. Volume analysis within the corpus callosum, SVZ and cortex at P4 & P21 demonstrated no significant difference

between the control and GMH pups indicating that the increase in ventricular volume was not due to parenchymal loss.

We have shown that the experimental model of moderate GMH we have developed, causes ventriculomegaly at P4 which persists up to P21, faithfully recapitulating a key feature of the human condition.

GMH causes increased proliferation in the wall of the lateral ventricle

To assess the impact of GMH on the NSPC within the SVZ we adopted a thymidine labelling strategy whereby five intraperitoneal injections, at 2 hourly intervals, were given on day one (P1) [29]. The number of EdU^{+ve} cells within the lateral wall of the lateral ventricle was quantified after 3 days and a significant increase was found in the GMH samples as compared to controls (Control (n=4) 57.5 ± 8.605, Sham (n=5) 80.23 ± 5.008, GMH (n=4) 165 ± 24.09, p=0.0008 ANOVA) (Figure2 A-B). Importantly, Sham injection did not elicit a similar effect, therefore excluding that the observed phenotype was due to the injection alone. EdU staining was found to be tightly confined to $DAPI^{+ve}$ nuclei, and no picnotic/apoptotic cells were seen in the wall of the lateral ventricle. The pattern of EdU staining was also seen to change from a solid high intensity signal in the control setting to a more fragmented and less intense signal in the GMH sample, implicating a dilution of the EdU signal secondary to increased proliferation (Figure 2A).

To determine if the increase in EdU^{+ve} cells could be accounted for by an increase in the number of transient amplifying (TAP) cells we co-stained for the nuclear marker MASH1 (ASCL1) which has been shown to be expressed at high levels in TAP[9]. This demonstrated a significant increase in the number of $MASH1^{+ve}$ cells within the wall of the lateral ventricle in the GMH samples (Control (n=4) 67 ± 10.24, GMH (n=4) 178 ± 27.84 p=0.0096 t-test) (Figure 2C,D-E). Staining for GFAP (gliogenic lineage) (Figure 2A,D-E) showed similar findings (Control (n=4) 97.79 ± 7.55, Sham (n=5) 160.2 ± 2.705, GMH (n=4) 265.9 ± 48.25, p=0.004 ANOVA). Colocalisation analysis revealed a significant increase in the number of cells colocalising MASH1 & EdU (Control (n=4) 9 ± 2.97, GMH (n=4) 29.5 ± 4.66, p=0.01 t-test) and in the number of cells colocalising GFAP & EdU (Control (n=4) 32.13 ± 5.23, Sham (n=5) 47.63 ± 3.5, GMH (n=4) 101.2 ± 19.69, p=0.004 ANOVA)

To exclude that the increase in the number of EdU^{+ve} cells within the SVZ could be accounted for by an infiltration of inflammatory cells, we stained for the microglial marker Iba1. We show that whilst a significant inflammatory response was elicited by blood injection as evidenced by the significant increase in the number of $Iba1^{+ve}$ cells counted within the SVZ following GMH (Control (n=4) 14 ± 2.35, GMH (n=4) 30.8 ± 5.1 p=0.02 t-test), this did not account for the significant rise in the number of EdU^{+ve} cells as the majority of the EdU^{+ve} cells were Iba1 negative (Figure S5).

In summary, we have shown that GMH causes an increase in the number of EdU^{+ve} cells within the wall of the lateral ventricle with a significant increase in the number of transient amplifying cells and glial cells.

GMH causes an increase in the number of $NG2^{+ve}$ progenitors within the corpus callosum

While carrying out the analysis within the lateral wall of the lateral ventricle as described above, it became apparent that increased numbers of EdU^{+ve} cells were also seen within the callosal / dorsal border of the ventricle, a finding which is also seen in the MASH1 staining (Figure 2C). This area is recognised by Suzuki et al [34] as a key postnatal gliogenic migratory pathway out of the SVZ and into the cortex (Figure 3A), as such to quantify this increase, analysis was undertaken within the corpus callosum on an independent series of sagittally sectioned brains (Figure 3 B-C).

The first most striking finding was that the blood-injected samples exhibited a different morphology within the corpus callosum. The normal perpendicular arrangement of cells was replaced by a markedly hypercellular and disordered pattern (Figure 3D). Quantification of the number of EdU^{+ve} cells, again demonstrated a significant increase following IC blood injection, which was not found in the sham control (Control (n=6) 32.73 ± 1.386, Sham (n=5) 35.03 ± 1.662, GMH (n=6) 49.09 ± 4.83, p=0.0049 ANOVA) (Figure 3E). Colocalisation revealed a significant increase in $NG2^{+ve}$ EdU^{+ve} cells (Control (n=6) 11.67 ± 2.362 GMH (n=6) 20.17 ± 1.558 p=0.013 t-test) with a trend for increase also seen in the $GFAP^{+ve}/EdU^{+ve}$ population whilst no increase was seen in the number of cells colocalising EdU & Dcx (Figure 4).

The corpus callosum is thought to represent a major conduit of glial progenitors migrating from the SVZ to the cortex [34]. Here we show that GMH not only impacts on the SVZ but also leads to an increase in the number of $NG2^{+ve}$ lineage committed progenitors in the corpus callosum.

Reduced expression of Olig2 at P21 after GMH

Given that we have shown that GMH causes phenotypic changes within the SVZ and the corpus callosum at an acute / immediate stage (P4) we resolved to determine how this might impact on early cortical development. To achieve this we analysed the neocortex from P21 mice as this was felt to be representative of juvenile brain development (Figure 5A).

We found that GMH causes a significant reduction in the percentage of EdU^{+ve} cells (Control (n=3) 13.66 ± 0.86, GMH (n=3) 9.88 ± 0.45 p=0.017 t-test) (Figure 5B) throughout the cortex and it was not limited to any specific layer. Co-staining with the panneuronal marker NeuN revealed that in the control setting less than 1% of the DAPI cells counted were found to be labelled for both EdU and NeuN and this was not found to be significantly affected by GMH (Figure 5C).

Further costaining with the oligodendrocyte marker Olig2 revealed that while in the control setting around 9% of cells were labelled with EdU and Olig2, this was seen to drop significantly to around 6% following GMH (Control (n=3) 8.54 ± 0.34, GMH (n=3) 6.07 ± 0.35, p=0.007 t-test) (Figure 5D). Similarly the percentage of cells that express Olig2 was seen to significantly decrease following GMH (Control (n=3) 12.69 ± 0.53, GMH (n=3) 9.63 ± 0.61, p= 0.019 t-test) (Figure 5E).

Taken together these data suggest that GMH has a negative impact on postnatal oligodendrogenesis while not significantly affecting postnatal neurogenesis. Whether this is due to direct toxicity or an impact on differentiation or migration of oligodendrocyte precursors remains to be definitively clarified.

Moderate GMH causes transient early impacts on neonatal development

Following IC blood injection at P0 we observed an increased number of falls (Control (n=15) 4.5 ± Sham (n=12) 9.33 ± GMH (n=21) 22.23 ± ANOVA) and significantly more fails in grip strength testing (Control (n=15) 1.875 ± Sham (n=12) 1.83 ± GMH (n=21) 2.47 ± ANNOVA) at P3 to P6 however this difference did not persist and in

contrary to published models of GMH (Aquilina [24], Xue [26], Lekic [25]) we found no persistent deficits / alterations in neuromotor development up to P21. (Figure S4). This finding differentiates our model as more representative of low grade GMH i.e. Papile grade II & III in contrast to the Grade IV haemorrhage modelled by those previously published [24-26]. This finding further reinforces the need for this model of low grade GMH and implies that the global impact of grade IV haemorrhage may mask the more subtle impact that GMH/IVH has on the NSPC within the SVZ.

GMH causes Notch down-regulation in CD133^{+ve} cells in the SVZ

Next, we set out to assess the impact of GMH on the molecular regulation within the proximal / ventricular domain. To this end MACS sorting of Prominin/CD133 labelled cells from a single hemisphere of P4 blood injected vs. control pups was carried out. Prominin is a transmembrane glycoprotein expressed by ependymal cells and on the primary cilia of NSPC [35] within the SVZ, its expression decreases through gestation but its expression is highly conserved within the ventricular / proximal domain at P4 [36].

Expression analysis of a selection of genes known to play a role in SVZ NSPC regulation was carried out on RNA extracted from the injured hemisphere of three animals and uninjured controls. Eight genes were found to be significantly deregulated with only Hsp90ab1 being up regulated and all others, Notch2, Ep300, Kat2a, Sox2, Cxcl12, Tubb3, and Ccne1 down regulated (Figure 6A).

Given the integral role that the Notch pathway has in modulating stem cell proliferation and differentiation, we were intrigued to find that Notch 2 expression was down regulated >25 fold following GMH. To validate these findings, in-situ-hybridisation for the Notch pathway effector Hes5 was used (Control n=3, GMH n=3). In the uninjured P4 SVZ, Hes5 is expressed in both the ependymal lining and in few scattered GFAP^{+ve} cells, as demonstrated by double staining for GFAP/Hes5 (Figure 5B). A striking reduction of Hes5 staining was observed in the SVZ of P4 mice following GMH in all the samples tested, particularly marked in the anterior SVZ (Figure 5C).

The observed down regulation of the Notch pathway in CD133^{+ve} cells in the SVZ after GMH raises the possibility that Notch signalling could be functionally mediating

the proliferative burst of TAP with subsequent aberrant differentiation observed in the mature cortex.

Discussion

Despite advances in perinatal care, EP is still a common cause of disability in children and GMH is the most prevalent intracranial lesion seen in premature babies [37]. Due to the multifactorial nature of the EP [23], isolating the impact of GMH and deciphering its effect on the NSPC and cortical development remains elusive.

The severity of haemorrhage correlates with outcome [38] and ranges from minor bleeds within the substance of the GM to significant life threatening haemorrhages, which extend into the ventricle causing florid hydrocephalus and associated venous infarction [39]. There is widespread agreement that outcome following high grade haemorrhage is poor [40] which is likely due in part to the destructive impact on the parenchyma[23]. However, outcome following moderate / low-grade haemorrhage is more variable with contradictory reports in the literature [41-43]. More advanced neuroimaging techniques have shown that even if development appears outwardly normal, functional MRI imaging following premature birth shows markedly abnormal connectivity and synchronisation [44,45] and volumetric analysis indicates reduced brain size and cortical gyration [46-49]. Postnatally developed neuronal cells [4] with reduced dendritic arborisation [45] are also increasingly recognised as important consequences of premature birth.

Given the clinical significance of GMH numerous models in different animal species have been trialled [50] however to date all models have focused on the severe end of the spectrum with extensive cortical injury where diffuse haemorrhage and marked disturbance in behaviour are seen [25,51,52] . It is well recognised that NSPC within the SVZ are exquisitely sensitive to microenvironmental cues [9,10] and further that haemorrhage within the ventricle alters the expression of NSC modulators, such as TGFβ [53]. As such in order to understand how GMH impacts on NSPC and cortical development in the intermediate group, in whom outcome appears to be most variable and who may have the most to gain from intervention, a more subtle injury model is needed. Currently available physiological techniques [52] cannot be used to model low grade GMH as it causes widespread haemorrhage within the brain parenchyma [50] and may also be confounded by the use of glycerol, which has been shown to

impact independently on cortical development [54]. Similarly the interpretation of results following the injection of collagenase into the SVZ [25], whilst reducing bolus size, is significantly limited due to the potentially confounding affect of collagenase on the NSPC.

Modelling intracerebral haemorrhage through targeted mutations within components of the blood brain barrier has been instrumental in determining the aetiology of GMH, for example the role of integrins [55], collagen [56] and pericytes [57] have all been shown. Further to this, using a tetracycline inducible system to initiate VEGF expression within the GM of the developing embryo, Yang et al have shown high rates of IVH [58]. The transgenic models developed to date invariably cause intrauterine bleeding and are associated with a high perinatal mortality, as such no widely accepted transgenic model of neonatal GMH has yet been developed to determine how postnatal haemorrhage impacts on cortical development.

We have chosen to use injection of autologous blood to circumvent the potentially misleading influence of using non-physiological substances. Similarly, reducing the volume of injection to 5ul and employing a stereotactic injection technique limits the kinetic impact of the blood bolus and focuses the lesion within the SVZ whilst limiting collateral damage to the surrounding parenchyma. The fact that stereotactic blood injection causes minimal primary damage to the cortex with low rates of porencephalic cyst formation, whilst accurately modelling ventriculomegaly and microglial activation reinforces the premise that the effect of GMH, in this model, is subtle and offers a unique opportunity to understand how moderate degrees of haemorrhage impact on the NSPC and cortical development.

Our primary finding of increased EdU^{+ve} cells in the wall of the lateral ventricle at P4 following GMH at P0, was initially unexpected given that a previous blood injection model had shown a reduction in proliferation following GMH [26]. This likely reflects the different degrees of haemorrhage modelled by the two approaches. The finding of activation of proliferation following GMH is in keeping with ischaemic models of premature brain injury [59], whilst differences may exist in the temporal course (delayed response seen following ischaemia and a more immediate response seen following haemorrhage), this finding suggests activation of a common pathway following brain injury in the premature neonate.

Co-staining within the SVZ at P4 revealed that the increase in EdU^{+ve} cells seen following GMH is in part accounted for by an increase in the number of $MASH1^{+ve}$ and $GFAP^{+ve}$ progenitor cells. Further to this, analysis of the postnatal gliogenic migratory pathway out of the SVZ [34] (i.e. within the corpus callosum) revealed a significant increase in the number of glial progenitors (EdU^{+ve} / $NG2^{+ve}$) following GMH/IVH. This combination of findings implicates that moderate grade GMH associated with intraventricular extension causes an activation of proliferation within the SVZ with a consequent increase in the number of glial progenitors within the postnatal migratory pathways.

Interestingly, by analysing the neocortex at P21 we find that this initial burst of proliferation of glial progenitors does not increase the proportion of glial cells within the cortex indeed the opposite is seen, with reduced numbers of $Olig2^{+ve}$ cells seen within the neocortex. This finding implies that the burst of glial progenitor cells produced by the activation of precocious proliferation within the SVZ (in reaction to GMH/IVH) are unable to integrate within the cortex and further to this that the developing cortex is unable to compensate for the loss of potential and abnormal temporal activation.

These intriguing findings led us to speculate that GMH may be impacting on the molecular control of NSC within the proximal / ventricular domain of the SVZ in our model. To address this question we decided to isolate cells from the proximal / ventricular domain of the neonatal pup using a CD133 MACS protocol. Whilst no single marker has been demonstrated to show absolute sensitivity and specificity, CD133 is a robust and widely accepted marker of ependymal cells and NSC in the early postnatal brain [30].

Expression analysis demonstrated that moderate grade GMH down regulates Notch2 within the $CD133^{+ve}$ cell fraction (Figure 6A). The periventricular location of Notch signalling down regulation following GMH was confirmed using in-situ-hybridisation directed against Hes5, a downstream effector of the Notch pathway (Figure 6C).

The role of the Notch signalling pathway in the maintenance and differentiation of SVZ NSC is well characterised. Evidence of activation of the pathway in quiescent NSC was shown in transgenic mice where the expression of a reporter gene was driven by the Hes5 promoter or RBPj binding sites and its main role was found to be

the maintenance of the pool of undifferentiated quiescent NSC [14]. In fact, conditional inactivation of the pathway led to a premature conversion of slowly dividing NSC into transient amplifying cells, a phenomenon accompanied by a proliferative burst which led to premature differentiation of the cells and to depletion of the pool of undifferentiated NSC as well as subsequent premature cessation of neurogenesis [14]. In our model of GMH, we found profound disruption of the SVZ including the ependymal lining and concomitant decrease of Notch activity as assessed by reduced numbers of cells expressing the Notch signalling downstream effector Hes5. It is conceivable that the decreased Notch signalling may be responsible for the proliferative burst of transient amplifying progenitors observed at P4. These data are in agreement with previous studies, where disruption of the ependymal cells by an ischaemic injury led to decreased Notch signalling, which in turn induced a fate change followed by cell cycle entry and neuronal differentiation [60]. We did not observe increased neuronal differentiation in our model at P21 but a decreased oligodendrogenesis instead, possibly because our injury strategy mainly affects the dorsal and anterior SVZ, an area where NSC with oligodendrocytic potential are enriched for [61]. These results are also in keeping with the reported role of Notch signalling in favouring oligodendrocytic specification [62]

Furthermore, Notch has an important role in dendritic arborisation of immature neurons in the adult brain, in fact conditional knock-out of Notch 1 results in significantly less complex arborisation, while overexpression of activated Notch 1 leads to a significant increase in dendritic complexity in newborn, maturing granule cells of the adult dentate gyrus [63]. Future studies will tell whether similar abnormalities are seen at later stages in our mouse model, since they could provide a preliminary explanation for subtler neurocognitive sequelae suffered by GMH patients later in their life.

It will be important to assess the translational value of these findings in human autoptic GMH brain tissue as Notch down regulation may represent a final common pathway following premature birth. Should this be the case, quantification of Notch expression in the GM may prove a useful prognostic indicator and importantly, pharmacological activation of the Notch pathway, which has been shown to be achievable and to exert the predicted functional impact in human cells [64,65], could be therapeutically pursued

Taken together these findings raise the possibility that activation of Notch signalling could be a therapeutic strategy for GMH and our mouse model would be an ideal platform to test this hypothesis at pre-clinical level.

Acknowledgements

We thank all members of the Marino Lab for helpful discussions. We are grateful to the BSU staff for help in the daily care of our mouse colony. This work is supported in part through grants from the British Neuropathological Society, The Royal College of Surgeons, SPARKS the Children's Medical Charity (11QMURTF13) and the Barts and London Charity (468/1739).

Figure legends

Figure 1. Stereotactic injection of autologous blood recapitulates moderate grade GMH (A) The Narishige stereotactic frame was modified with a clay mould (inset) secured to a custom made board shaped to fit the space into which the proprietary metal plate would ordinarily sit. The board is secured down using the housing screws shown and in combination with the taping shown in **(B)** this method facilitates reproducible immobilisation of the P0 mouse pup. **(C)** (i) Schematic showing the point of bolus injection within the anterior margin of the SVZ (ii) Macroscopic picture showing the result of tissue dye injection into the SVZ – a small entry wound and needle tract can be seen leading to the injection bolus within the anterior SVZ, bilateral intraventricular spread can also be clearly seen (iii) Matching macroscopic picture showing the result of blood injection into the SVZ a tiny entry wound with a very similar distribution of intraventricular blood can be seen, the relative lack of surrounding tissue damage and the absence of any subdural blood is also noted. **(D)** Coronal section of day 1(P1) mouse brain stained with H&E (i) x5 magnification and (ii) x10 magnification, following stereotactic blood injection on the day of birth (P0) demonstrating haematoma within the SVZ *(white arrow)* in association with intraventricular blood *(red arrow).* Minimal damage to the surrounding cortex is noted **(E)** Coronal section of day 4 (P4) mouse brain stained with H&E, (i) x10 magnification and (ii) x40, demonstrating haematoma cavity within the SVZ *(black arrow)* associated with the presence of siderophages *(green arrows).* **(F)** Graph showing that GMH causes ventriculomegaly at P4, (Control n=7, Sham n=4, GMH n=5 $p<0.05$ ANOVA) **(G)** Similarly at P21 we see a persistence of ventriculomegaly (Control n=5 GMH n=4 $p<0.05$ t-test) **(H)** The persistence of hydrocephalus following GMH can be seen at P21 in the small stature and marked doming of the

cranium (*inset top*: comparison of control pup; upper frame labelled **a**, with GMH pup; lower frame labelled **b**, demonstrates small stature at P21 in GMH pups, *inset bottom*: coronal view of brain with dilated lateral ventricles).

Figure 2 GMH activates proliferation in the wall of the lateral ventricle and increases the expression of GFAP and the number of MASH1^{+ve} cells (A) 40X Oil Confocal acquired tile scan images of the left lateral ventricle of the P4 mouse pup, comparing control (i&ii) versus blood injected/GMH (iii & iv) samples (DAPI-Blue GFAP-Red EdU-Green). In the control setting we see occasional EdU^{+ve} cells in the SVZ with minimal GFAP positivity, in the GMH sample we see a marked increase in the number of EdU^{+ve} cells *(white arrow)* with a marked increase in GFAP immunoreactivity. Marked ventriculomegaly is also seen in the GMH sample **(B)** Quantification of the number of EdU^{+ve} cells within the lateral and dorsal wall of the left lateral ventricle at P4 shows that GMH causes a significant increase in the number of cells counted in comparison to both the control and sham needle only conditions (Control n=4, Sham n=5, GMH n=4 $p<0.001$ ANNOVA) **(C)** Following GMH (iii&iv) we see a significant increase in the number of MASH1^{+ve} cells in the superior, medial and lateral walls of the lateral ventricle in comparison to control (i&ii) (DAPI-blue, MASH1-red) **(D)** Bar chart highlighting the increase in the number of MASH1^{+ve} and GFAP^{+ve} cells in the lateral wall of the left lateral ventricle following GMH compared to the control (Control n=4 GMH n=4: $p<0.01$ MASH1 $p<0.05$ GFAP t-test). **(E)** Bar Chart showing the significant increase in GFAP^{+ve}/EdU^{+ve} and MASH1^{+ve}/EdU^{+ve} cells following GMH (Control n=4 GMH n=4: $p<0.05$ MASH1 $p<0.05$ GFAP (scale bar 100µm)

Figure 3 GMH leads to an increase in the number of EdU^{+ve} transient amplifying cells within the corpus callosum (A) Sagittal schematic representation of the P4 mouse brain demonstrating the postnatal migratory patterns out of the SVZ (adapted from Suzuki et al 2003[34]), neuronal migration into the olfactory bulb is shown in green whilst glial migratory pathways are shown in yellow and orange **(B)** Sagittal single channel DAPI image from a P4 mouse pup to demonstrate the positioning of the 300 pixel wide counting frame *(white checkered box)* orientated anterior to a line drawn perpendicular to the anterior border of the hippocampus *(red arrow)* **(C)** Example of the counting frame used for quantification in the sagittal analysis (i) Single channel DAPI image demonstrates four phenotypically different regions; the subventricular zone (SVZ), corpus callosum (CC), subcortical white matter (SCWM)

649 and the cortex (CTX), quantification was undertaken within the CC (ii) Myelin Basic
650 Protein (MBP) (Green) staining used to demonstrate the anatomical boundaries
651 between the SCWM and CC facilitating quantification within the CC. **(D)** 40X oil tile
652 scans (DAPI-Blue EdU-Green) following GMH shows that the cellular architecture
653 within the CC is abnormal with markedly increased cellularity and a loss of the
654 perpendicular arrangement of nuclei (as seen in the control samples). Similarly we see
655 a significant increase in the number of EdU^{+ve} cells within the SVZ and CC whilst the
656 SCWM and CTX remain relatively unaffected **(E)** Quantification of the number of
657 EdU^{+ve} cells within the counting frame of the CC reveals that GMH causes a
658 significant increase in the number of EdU^{+ve} cells. (Control n=6 Sham n=5 GMH n=6
659 $p<0.01$ ANNOVA) (scale bar 100µm)
660
661 **Figure 4 GMH causes an increase in glial progenitors within the corpus callosum**
662 **(A)** Quantification of the number of cells which colocalise (i) GFAP (ii) NG2 & (iii)
663 Dcx reveals that GMH causes a significant increase in the number of cells which
664 colocalise EdU & NG2 with a similar trend seen in the number of cells colocalising
665 EdU & GFAP, with no comparative increase seen in the number of cells colocalising
666 EdU & Dcx **(B)** Representative example showing that GMH causes an increase in the
667 number of cells which colocalise EdU & NG2. (scale bar 100µm)
668
669 **Figure 5 GMH at P0 impacts on early cortical development (quantified at P21)**
670 **(A)** Quantification was undertaken in the neocortex anterior to a line drawn
671 perpendicular to anterior border of the hippocampus (area shaded in red). **(B)** GMH at
672 P0 significantly reduces the percentage of cells which express EdU within the cortex
673 at P21 (Control n=3 GMH n=3 $p<0.05$ t-test) **(C)** No significant change is seen in the
674 % of cells which colocalise EdU & NeuN (Control n=3 GMH n=3 $p=0.1$ t-test) **(D)** In
675 contrast analysis of colocalisation with markers of oligodendrocytic lineage reveals
676 that GMH significantly reduces the proportion of cells which colocalise EdU & Olig2
677 (Control n=3 GMH n=3 $p<0.01$ t-test) **(E)** Similarly, following GMH at P0 we see a
678 significant reduction in the percentage of cells which express the Oligodendrocyte
679 marker Olig2 (Control n=3 GMH n=3 $p<0.05$ t-test)
680
681 **Figure 6 GMH causes a down regulation of Notch2 in CD133 positive cells within**
682 **the wall of the lateral ventricle (A)** RNA analysis from the $CD133^{+ve}$ cell fraction
683 isolated from the wall of the lateral ventricle reveals that GMH causes a significant
684 down regulation of Ccne1, Cxcl12, Ep300, Kat2a, Notch2, Sox2, Tubb3 and

significant upregulation of Hsp90ab1 (Control n=3 GMH n=3 p-values shown in table calculated using t-test) **(B)** By overlaying the Hes5 ISH with the GFAP/EdU IHC we confirm the expression of Notch within the wall of the lateral ventricle predominantly in $GFAP^{-ve}$ cells with occasional expression in $GFAP^{+ve}$ cells **(C)** Photomicrographs showing in situ hybridisation performed using a Hes5 probe[32] on coronal sectioned P4 mouse brain. Specific localisation of the Hes5 probe to the wall of the lateral ventricle in the control setting is clearly seen (i&ii) with a significant reduction in Hes5 expression seen following GMH (iii & iv).

Supplementary data legends

Supplementary Figure 1 *Stereotactic injection facilitates accurate and reproducible targeting of the neonatal mouse SVZ with high rates of intraventricular extension and low rates of subdural extension* **(A)** Schematic demonstrating how the degree of angulation refers to the angle generated between the needle and an imaginary line drawn perpendicularly to the head of the mouse pup, in the example shown two angulations are depicted at 20^0 *(red needle)* and at 45^0 *(green needle)* **(B)** Chart showing the relative incidence of subdural (SD) and intraventricular extension of bleed (IVH) at macroscopic examination on day 4 following IC blood injection at P0 using the different trajectories of forward angulation. At 24 degrees of angulation we see a very low rate of subdural extension with high rates of intraventricular extension **(C-F)** Unstained coronal sections taken from P0 mouse brain following stereotactic tissue dye injection highlighting the location of the injection bolus (white circle) at the different trajectories trialled **(C)** 25^0 forward angulation, blood bolus is seen within parenchyma with intraventricular spread **(D)** 27^0 forward angulation bolus - site more lateral but IV spread still seen **(E)** 28^0 forward angulation, injection site is seen laterally with evidence of SD extension **(F)** 30^0 forward angulation, lateral injection site with SD extension. The reproducibility in the height of the injection bolus on the ventral dorsal axis is noted in association with the limited amount of surrounding damage to the brain parenchyma.

Supplementary Figure 2 *Anatomical landmarks used to identify the coronal zero specimens.* In order to facilitate robust comparison of volumetric measurements, quantification was undertaken between fixed anterior and posterior landmarks **(A-D)** Nissl stained coronal samples from P4 mouse pup x5 magnification **(A)** Penultimate slide prior to the anterior 'zero specimen' (i.e. zero minus 10μm) the continuity of the

corpus callosum is seen to be interrupted by the two parallel lines which constitute the indusium griseum (IG) the orientation of this structure can be taken as an indication of how 'square' the sample has been cut **(B)** *Anterior zero specimen* showing the corpus callosum in continuity across the midline (CC) this appearance demarcates the anterior extent of the region of quantification **(C)** Penultimate section prior to the posterior 'zero specimen' (zero minus 10μm) demonstrating that the fibres of the hippocampus do not cross the midline **(D)** *Posterior zero specimen*, fibres of the hippocampus are seen to cross the midline (white arrow) this appearance demarcates the posterior extent of the region of quantification **(E)** Schematic showing the orientation of the 'zero specimens' (anterior, posterior and sagittal) through the P4 mouse brain **(F)** Graph showing that the number of sequential 10um specimens collected between the anterior and posterior borders does not significantly change following blood injection, facilitating comparison of the volumetric analysis using these landmarks described above.

Supplementary Figure 3 *Anatomical landmarks used to identify the sagittal zero specimens* - In order to facilitate robust comparison of specimens from control and blood injected samples in the sagittal plane we used the first appearance of striations of the caudate putamen within the rostral migratory stream to denote the sagittal zero specimen **(A-F)** Unstained sagittal sections of P4 brain as viewed at the cryostat to determine the zero slide **(A&B)** Samples one and two sections medial to the zero slide respectively demonstrating an intact SVZ and RMS with no evidence of the striations of the caudate putamen **(C)** *Sagittal zero slide* – the last slide in which the striations of the caudate putamen are not visible **(D&E)** First and second samples lateral to the sagittal zero respectively, showing the emergence of the striations, consistent with the caudate putamen, within the SVZ **(F)** High power field taken from the Zero specimen showing the lateral ventricle and SVZ / RMS, with no evidence of the striations consistent with the caudate putamen.

Supplementary Figure 4 *GMH elicits an inflammatory response in the wall of the lateral ventricle but this does not account for the significant increase in* EdU^{+ve} *cells* Graph showing a significant increase in the number of cells expressing Iba1 in pups following GMH.

Supplementary Figure 5 *GMH at P0 causes early changes in grip strength and propensity to fall but does not cause lasting neuromotor deficit* **(A&B)** Screen shots

taken showing the technique used to test grip strength, the paws are placed onto a piano wire and the pups ability to grip for more than 5 seconds is recorded **C** Graph showing the number of failed attempts at grip strength testing – analysis reveals that GMH causes significantly more failed attempts at 4 to 6 days **(D-F)** Screen shots detailing the technique used for negative geotaxis, the pup is placed head down on a surface inclined at 45^0 and the time taken to turn 180^0 recorded. Testing time is limited to 30 seconds **G** Graph showing that GMH does not significantly impact on negative geotaxis **(H-J)** Screen shots to show the technique used to assess surface righting; the pup is rolled onto its back and the time taken to stand on all four paws is recorded. Testing time limited to 30 seconds **K** Graph showing the time taken for surface righting, no significant impact of GMH on time to surface right is seen. **L** Analysis of the number of falls recorded demonstrates that GMH is associated with significantly more falls at 4 to 6 days **M** Graph showing the total time mobile (secs) within the testing chamber – no significant change was seen following GMH **N** Graph showing the total distance travelled within the testing chamber –at 19 to 21 days needle injection (i.e. sham and GMH) is seen to cause a significant increase in the total distance travelled **O** Graph showing the maximum speed recorded whilst in the testing chamber – a significant increase in the total maximum speed is seen at 13 to 15 days following GMH.

References

1 Chang HH, Larson J, Blencowe H, Spong CY, Howson CP, Cairns-Smith S, Lackritz EM, Lee SK, Mason E, Serazin AC: Preventing preterm births: analysis of trends and potential reductions with interventions in 39 countries with very high human development index. The Lancet 2013;381:223-234.

2 Goldenberg RL, Culhane JF, Iams JD, Romero R: Epidemiology and causes of preterm birth. The lancet 2008;371:75-84.

3 Ballabh P: Intraventricular hemorrhage in premature infants: mechanism of disease. Pediatric research 2010;67:1-8.

4 Back SA: Brain Injury in the Preterm Infant: New Horizons for Pathogenesis and Prevention. Pediatric Neurology 2015

5 Fleiss B, Gressens P: Tertiary mechanisms of brain damage: a new hope for treatment of cerebral palsy? Lancet Neurol 2012;11:556-566.

6 Hack M, Wilson-Costello D, Friedman H, Taylor GH, Schluchter M, Fanaroff AA: Neurodevelopment and predictors of outcomes of children with birth weights of less than 1000 g: 1992-1995. Archives of pediatrics & adolescent medicine 2000;154:725-731.

7 Vohr BR, Wright LL, Poole WK, McDonald SA: Neurodevelopmental outcomes of extremely low birth weight infants< 32 weeks' gestation between 1993 and 1998. Pediatrics 2005;116:635-643.

8 Wood N, Costeloe K, Gibson A, Hennessy E, Marlow N, Wilkinson A: The EPICure study: associations and antecedents of neurological and developmental

disability at 30 months of age following extremely preterm birth. Arch Dis Child-Fetal Neonatal Ed 2005;90:F134-F140.
9 Tong CK, Alvarez-Buylla A: SnapShot: adult neurogenesis in the V-SVZ. Neuron 2014;81:220-220 e221.
10 Fuentealba LC, Obernier K, Alvarez-Buylla A: Adult Neural Stem Cells Bridge Their Niche. Cell Stem Cell 2012;10:698-708.
11 Lehtinen MK, Zappaterra MW, Chen X, Yang YJ, Hill AD, Lun M, Maynard T, Gonzalez D, Kim S, Ye P, D'Ercole AJ, Wong ET, LaMantia AS, Walsh CA: The cerebrospinal fluid provides a proliferative niche for neural progenitor cells. Neuron 2011;69:893-905.
12 Lim DA, Tramontin AD, Trevejo JM, Herrera DG, García-Verdugo JM, Alvarez-Buylla A: Noggin antagonizes BMP signaling to create a niche for adult neurogenesis. Neuron 2000;28:713-726.
13 Kopan R, Ilagan MXG: The canonical Notch signaling pathway: unfolding the activation mechanism. Cell 2009;137:216-233.
14 Imayoshi I, Sakamoto M, Yamaguchi M, Mori K, Kageyama R: Essential roles of Notch signaling in maintenance of neural stem cells in developing and adult brains. J Neurosci 2010;30:3489-3498.
15 Liu X, Wang Q, Haydar TF, Bordey A: Nonsynaptic GABA signaling in postnatal subventricular zone controls proliferation of GFAP-expressing progenitors. Nature neuroscience 2005;8:1179-1187.
16 Shen Q, Goderie SK, Jin L, Karanth N, Sun Y, Abramova N, Vincent P, Pumiglia K, Temple S: Endothelial cells stimulate self-renewal and expand neurogenesis of neural stem cells. Science 2004;304:1338-1340.
17 Sanai N, Nguyen T, Ihrie RA, Mirzadeh Z, Tsai HH, Wong M, Gupta N, Berger MS, Huang E, Garcia-Verdugo JM, Rowitch DH, Alvarez-Buylla A: Corridors of migrating neurons in the human brain and their decline during infancy. Nature 2011;478:382-386.
18 Paredes MF, James D, Gil-Perotin S, Kim H, Cotter JA, Ng C, Sandoval K, Rowitch DH, Xu D, McQuillen PS: Extensive migration of young neurons into the infant human frontal lobe. Science 2016;354:aaf7073.
19 Ernst A, Alkass K, Bernard S, Salehpour M, Perl S, Tisdale J, Possnert G, Druid H, Frisén J: Neurogenesis in the striatum of the adult human brain. Cell 2014;156:1072-1083.
20 Kriegstein A, Alvarez-Buylla A: The glial nature of embryonic and adult neural stem cells. Annu Rev Neurosci 2009;32:149-184.
21 Menn B, Garcia-Verdugo JM, Yaschine C, Gonzalez-Perez O, Rowitch D, Alvarez-Buylla A: Origin of oligodendrocytes in the subventricular zone of the adult brain. J Neurosci 2006;26:7907-7918.
22 Back SA, Luo NL, Borenstein NS, Levine JM, Volpe JJ, Kinney HC: Late oligodendrocyte progenitors coincide with the developmental window of vulnerability for human perinatal white matter injury. J Neurosci 2001;21:1302-1312.
23 Volpe JJ: Brain injury in premature infants: a complex amalgam of destructive and developmental disturbances. Lancet Neurol 2009;8:110-124.
24 Aquilina K, Chakkarapani E, Love S, Thoresen M: Neonatal rat model of intraventricular haemorrhage and post-haemorrhagic ventricular dilatation with long-term survival into adulthood. Neuropathol Appl Neurobiol 2011;37:156-165.
25 Lekic T, Manaenko A, Rolland W, Krafft PR, Peters R, Hartman RE, Altay O, Tang J, Zhang JH: Rodent neonatal germinal matrix hemorrhage mimics the human brain injury, neurological consequences, and post-hemorrhagic hydrocephalus. Exp Neurol 2012;236:69-78.
26 Xue M, Balasubramaniam J, Buist RJ, Peeling J, Del Bigio MR: Periventricular/intraventricular hemorrhage in neonatal mouse cerebrum. J Neuropathol Exp Neurol 2003;62:1154-1165.

27 Alles YC, Greggio S, Alles RM, Azevedo PN, Xavier LL, DaCosta JC: A novel preclinical rodent model of collagenase-induced germinal matrix/intraventricular hemorrhage. Brain Res 2010;1356:130-138.
28 Merkle FT, Mirzadeh Z, Alvarez-Buylla A: Mosaic organization of neural stem cells in the adult brain. Science 2007;317:381-384.
29 Inta D, Alfonso J, von Engelhardt J, Kreuzberg MM, Meyer AH, van Hooft JA, Monyer H: Neurogenesis and widespread forebrain migration of distinct GABAergic neurons from the postnatal subventricular zone. Proceedings of the National Academy of Sciences of the United States of America 2008;105:20994-20999.
30 Pfenninger CV, Roschupkina T, Hertwig F, Kottwitz D, Englund E, Bengzon J, Jacobsen SE, Nuber UA: CD133 is not present on neurogenic astrocytes in the adult subventricular zone, but on embryonic neural stem cells, ependymal cells, and glioblastoma cells. Cancer research 2007;67:5727-5736.
31 Bolos V, Grego-Bessa J, de la Pompa JL: Notch signaling in development and cancer. Endocr Rev 2007;28:339-363.
32 Muzio L, Soria J, Pannese M, Piccolo S, Mallamaci A: A mutually stimulating loop involving emx2 and canonical wnt signalling specifically promotes expansion of occipital cortex and hippocampus. Cerebral Cortex 2005;15:2021-2028.
33 Fancy SP, Harrington EP, Yuen TJ, Silbereis JC, Zhao C, Baranzini SE, Bruce CC, Otero JJ, Huang EJ, Nusse R: Axin2 as regulatory and therapeutic target in newborn brain injury and remyelination. Nature neuroscience 2011;14:1009-1016.
34 Suzuki SO, Goldman JE: Multiple cell populations in the early postnatal subventricular zone take distinct migratory pathways: a dynamic study of glial and neuronal progenitor migration. J Neurosci 2003;23:4240-4250.
35 Codega P, Silva-Vargas V, Paul A, Maldonado-Soto AR, DeLeo AM, Pastrana E, Doetsch F: Prospective identification and purification of quiescent adult neural stem cells from their in vivo niche. Neuron 2014;82:545-559.
36 Olausson KH, Maire CL, Haidar S, Ling J, Learner E, Nistér M, Ligon KL: Prominin-1 (CD133) defines both stem and non-stem cell populations in CNS development and gliomas. PloS one 2014;9:e106694.
37 Brouwer A, Groenendaal F, van Haastert IL, Rademaker K, Hanlo P, de Vries L: Neurodevelopmental outcome of preterm infants with severe intraventricular hemorrhage and therapy for post-hemorrhagic ventricular dilatation. J Pediatr 2008;152:648-654.
38 Bassan H, Limperopoulos C, Visconti K, Mayer DL, Feldman HA, Avery L, Benson CB, Stewart J, Ringer SA, Soul JS, Volpe JJ, du Plessis AJ: Neurodevelopmental outcome in survivors of periventricular hemorrhagic infarction. Pediatrics 2007;120:785-792.
39 Papile L-A, Burstein J, Burstein R, Koffler H: Incidence and evolution of subependymal and intraventricular hemorrhage: A study of infants with birth weights less than 1,500 gm. The Journal of Pediatrics 1978;92:529-534.
40 Whitelaw A: Periventricular hemorrhage: a problem still today. Early Hum Dev 2012;88:965-969.
41 Patra K, Wilson-Costello D, Taylor HG, Mercuri-Minich N, Hack M: Grades I-II intraventricular hemorrhage in extremely low birth weight infants: Effects on neurodevelopment. The Journal of Pediatrics 2006;149:169-173.
42 O'shea TM, Allred EN, Kuban KCK, Hirtz D, Specter B, Durfee S, Paneth N, Leviton A, Investigators ES: Intraventricular Hemorrhage and Developmental Outcomes at 24 Months of Age in Extremely Preterm Infants. Journal of Child Neurology 2012;27:22-29.
43 Inder TE: Neurodevelopmental impact of low-grade intraventricular hemorrhage in very preterm infants. Journal of Pediatrics 2006;149:152-154.

906 44 Molnár Z, Rutherford M: Brain Maturation After Preterm Birth. Science
907 translational medicine 2013;5:168ps162.
908 45 Dean JM, McClendon E, Hansen K, Azimi-Zonooz A, Chen K, Riddle A,
909 Gong X, Sharifnia E, Hagen M, Ahmad T: Prenatal cerebral ischemia disrupts MRI-
910 defined cortical microstructure through disturbances in neuronal arborization. Science
911 translational medicine 2013;5:168ra167-168ra167.
912 46 Dubois J, Benders M, Cachia A, Lazeyras F, Leuchter RH-V, Sizonenko S,
913 Borradori-Tolsa C, Mangin J, Hüppi PS: Mapping the early cortical folding process in
914 the preterm newborn brain. Cerebral Cortex 2008;18:1444-1454.
915 47 Toft PB, Leth H, Ring PB, Peitersen B, Lou HC, Henriksen O: Volumetric
916 analysis of the normal infant brain and in intrauterine growth retardation. Early
917 human development 1995;43:15-29.
918 48 Tolsa CB, Zimine S, Warfield SK, Freschi M, Rossignol AS, Lazeyras F,
919 Hanquinet S, Pfizenmaier M, Hüppi PS: Early alteration of structural and functional
920 brain development in premature infants born with intrauterine growth restriction.
921 Pediatric research 2004;56:132-138.
922 49 Jary S, De Carli A, Ramenghi LA, Whitelaw A: Impaired brain growth and
923 neurodevelopment in preterm infants with posthaemorrhagic ventricular dilatation.
924 Acta Paediatr 2012;101:743-748.
925 50 Balasubramaniam J, Del Bigio MR: Animal models of germinal matrix
926 hemorrhage. J Child Neurol 2006;21:365-371.
927 51 Balasubramaniam J, Xue M, Buist RJ, Ivanco TL, Natuik S, Del Bigio MR:
928 Persistent motor deficit following infusion of autologous blood into the
929 periventricular region of neonatal rats. Exp Neurol 2006;197:122-132.
930 52 Chua CO, Chahboune H, Braun A, Dummula K, Chua CE, Yu J, Ungvari Z,
931 Sherbany AA, Hyder F, Ballabh P: Consequences of intraventricular hemorrhage in a
932 rabbit pup model. Stroke 2009;40:3369-3377.
933 53 Whitelaw A, Christie S, Pople I: Transforming growth factor-beta1: a possible
934 signal molecule for posthemorrhagic hydrocephalus? Pediatric research 1999;46:576-
935 580.
936 54 Traudt CM, McPherson RJ, Studholme C, Millen KJ, Juul SE: Systemic
937 glycerol decreases neonatal rabbit brain and cerebellar growth independent of
938 intraventricular hemorrhage. Pediatric research 2014;75:389-394.
939 55 McCarty JH, Monahan-Earley RA, Brown LF, Keller M, Gerhardt H, Rubin
940 K, Shani M, Dvorak HF, Wolburg H, Bader BL: Defective associations between
941 blood vessels and brain parenchyma lead to cerebral hemorrhage in mice lacking αv
942 integrins. Molecular and Cellular Biology 2002;22:7667-7677.
943 56 Gould DB, Phalan FC, Breedveld GJ, van Mil SE, Smith RS, Schimenti JC,
944 Aguglia U, van der Knaap MS, Heutink P, John SW: Mutations in Col4a1 cause
945 perinatal cerebral hemorrhage and porencephaly. Science 2005;308:1167-1171.
946 57 Lindahl P, Johansson BR, Levéen P, Betsholtz C: Pericyte loss and
947 microaneurysm formation in PDGF-B-deficient mice. Science 1997;277:242-245.
948 58 Yang D, Baumann JM, Sun Y-Y, Tang M, Dunn RS, Akeson AL, Kernie SG,
949 Kallapur S, Lindquist DM, Huang EJ: Overexpression of vascular endothelial growth
950 factor in the germinal matrix induces neurovascular proteases and intraventricular
951 hemorrhage. Science translational medicine 2013;5:193ra190-193ra190.
952 59 Fagel DM, Ganat Y, Silbereis J, Ebbitt T, Stewart W, Zhang H, Ment LR,
953 Vaccarino FM: Cortical neurogenesis enhanced by chronic perinatal hypoxia. Exp
954 Neurol 2006;199:77-91.
955 60 Carlen M, Meletis K, Goritz C, Darsalia V, Evergren E, Tanigaki K,
956 Amendola M, Barnabe-Heider F, Yeung MS, Naldini L, Honjo T, Kokaia Z,
957 Shupliakov O, Cassidy RM, Lindvall O, Frisen J: Forebrain ependymal cells are
958 Notch-dependent and generate neuroblasts and astrocytes after stroke. Nat Neurosci
959 2009;12:259-267.

61 Ortega F, Gascón S, Masserdotti G, Deshpande A, Simon C, Fischer J, Dimou L, Lie DC, Schroeder T, Berninger B: Oligodendrogliogenic and neurogenic adult subependymal zone neural stem cells constitute distinct lineages and exhibit differential responsiveness to Wnt signalling. Nature cell biology 2013;15:602-613.
62 Zhou Q, Choi G, Anderson DJ: The bHLH transcription factor Olig2 promotes oligodendrocyte differentiation in collaboration with Nkx2. 2. Neuron 2001;31:791-807.
63 Breunig JJ, Silbereis J, Vaccarino FM, Sestan N, Rakic P: Notch regulates cell fate and dendrite morphology of newborn neurons in the postnatal dentate gyrus. Proc Natl Acad Sci U S A 2007;104:20558-20563.
64 Lobry C, Ntziachristos P, Ndiaye-Lobry D, Oh P, Cimmino L, Zhu N, Araldi E, Hu W, Freund J, Abdel-Wahab O: Notch pathway activation targets AML-initiating cell homeostasis and differentiation. The Journal of experimental medicine 2013;210:301-319.
65 Kannan S, Sutphin RM, Hall MG, Golfman LS, Fang W, Nolo RM, Akers LJ, Hammitt RA, McMurray JS, Kornblau SM: Notch activation inhibits AML growth and survival: a potential therapeutic approach. The Journal of experimental medicine 2013;210:321-337.

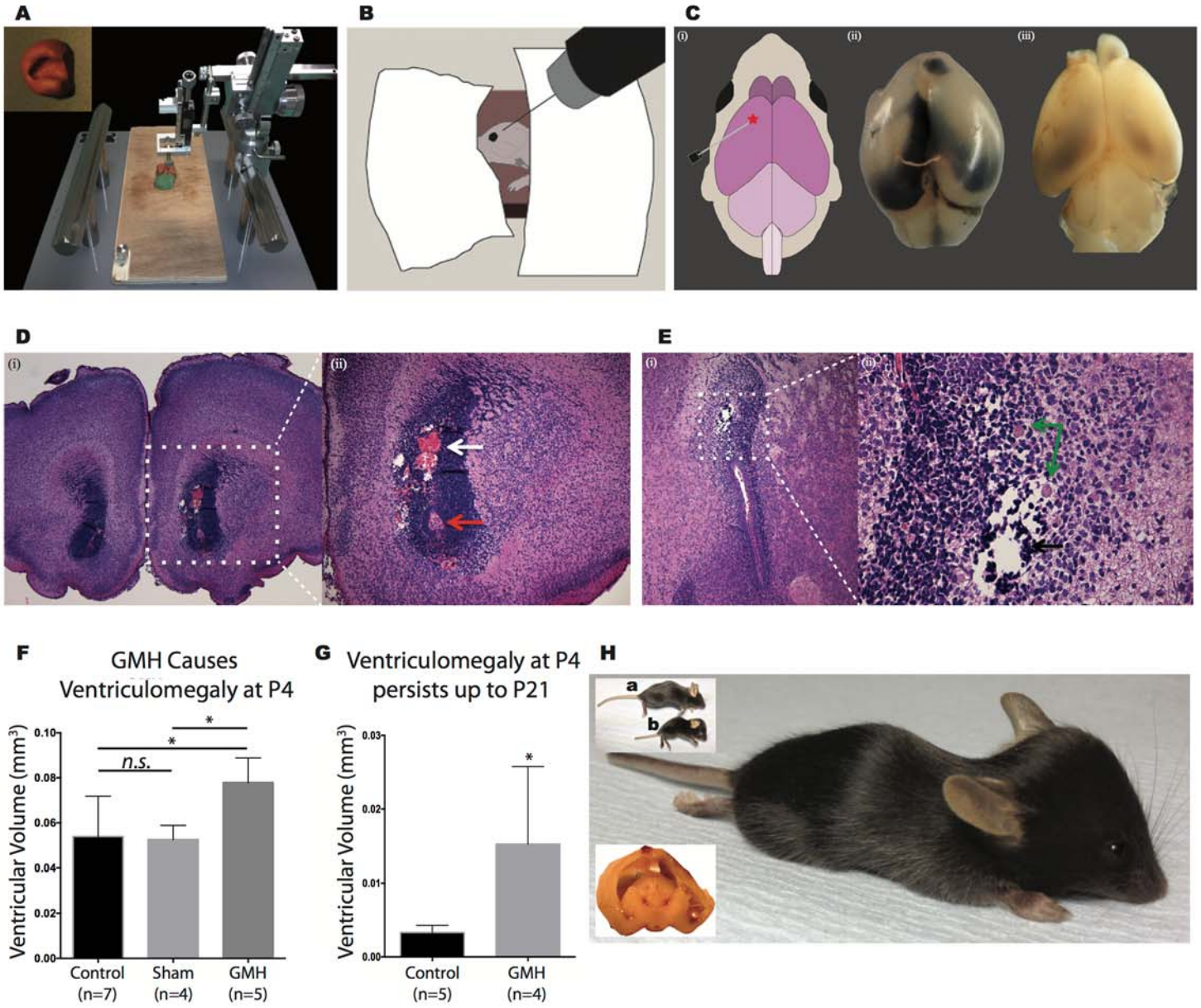
A
B
C
(i)
(ii)
(iii)
D
(i)
(ii)
E
(i)
(ii)
F
GMH Causes Ventriculomegaly at P4
Ventricular Volume (mm3)
0.10
0.08
0.06
0.04
0.02
0.00
*
*
n.s.
Control (n=7)
Sham (n=4)
GMH (n=5)
G
Ventriculomegaly at P4 persists up to P21
Ventricular Volume (mm3)
0.03
0.02
0.01
0.00
*
Control (n=5)
GMH (n=4)
H
a
b

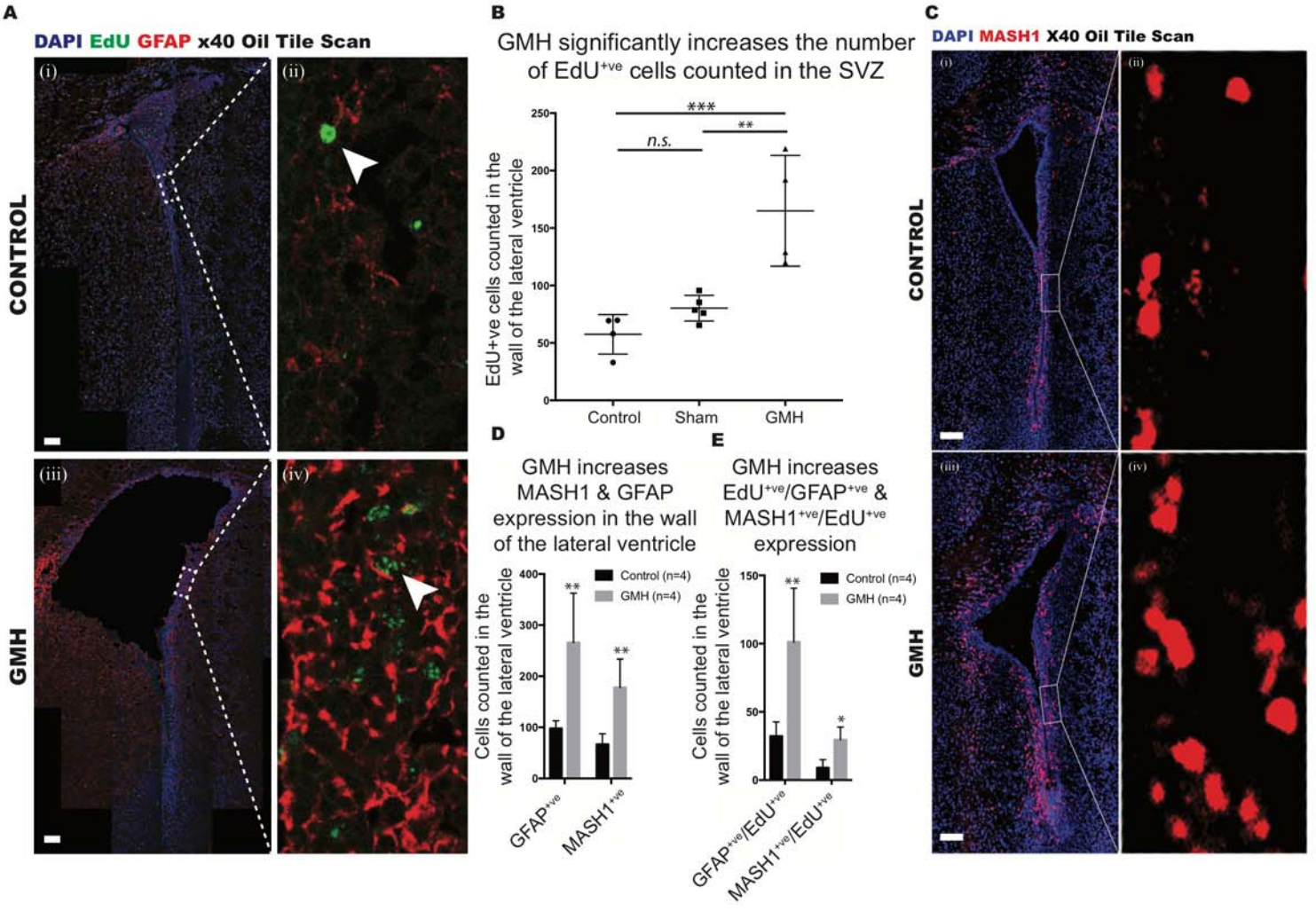
A
DAPI EdU GFAP x40 Oil Tile Scan
CONTROL
GMH
(i)
(ii)
(iii)
(iv)
B
GMH significantly increases the number of EdU+ve cells counted in the SVZ
EdU+ve cells counted in the wall of the lateral ventricle
250
200
150
100
50
0
***
**
n.s.
Control
Sham
GMH
C
DAPI MASH1 X40 Oil Tile Scan
CONTROL
GMH
(i)
(ii)
(iii)
(iv)
D
GMH increases MASH1 & GFAP expression in the wall of the lateral ventricle
Cells counted in the wall of the lateral ventricle
400
300
200
100
0
Control (n=4)
GMH (n=4)
**
**
GFAP+ve
MASH1+ve
E
GMH increases EdU+ve/GFAP+ve & MASH1+ve/EdU+ve expression
Cells counted in the wall of the lateral ventricle
150
100
50
0
Control (n=4)
GMH (n=4)
**
*
GFAP+ve/EdU+ve
MASH1+ve/EdU+ve

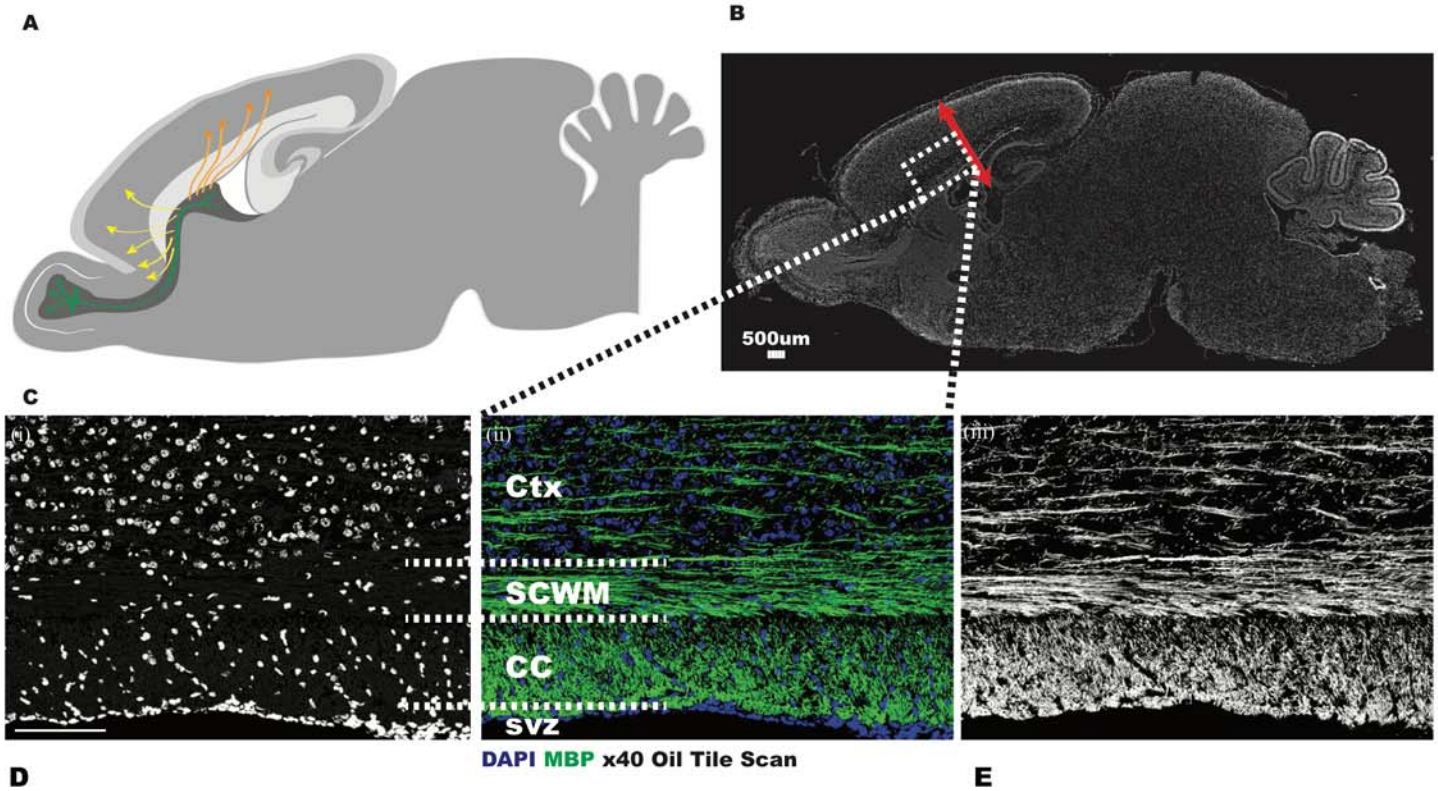
A
B
500um
C
(i)
(ii)
Ctx
SCWM
CC
SVZ
(iii)
DAPI MBP x40 Oil Tile Scan

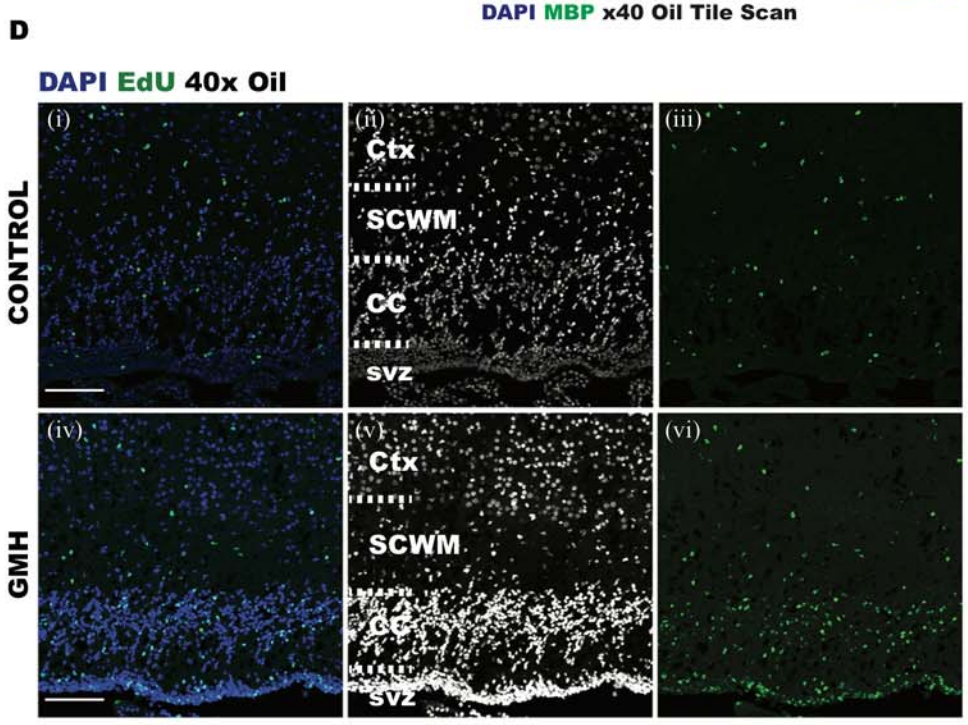
D
DAPI EdU 40x Oil
CONTROL
GMH
(i)
(ii)
Ctx
SCWM
CC
SVZ
(iii)
(iv)
(v)
Ctx
SCWM
CC
SVZ
(vi)

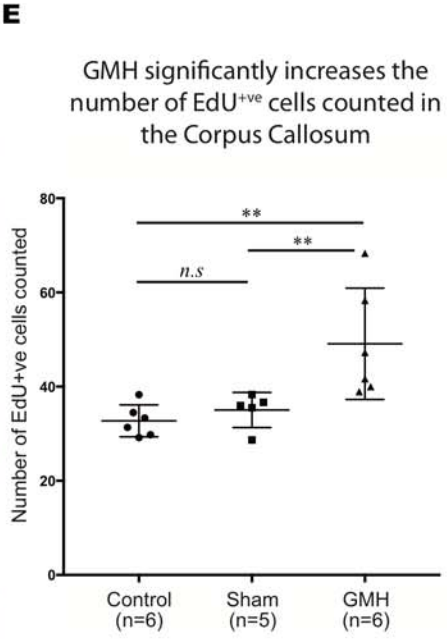
E
GMH significantly increases the number of EdU+ve cells counted in the Corpus Callosum
Number of EdU+ve cells counted
80
60
40
20
0
**
**
n.s
Control (n=6)
Sham (n=5)
GMH (n=6)

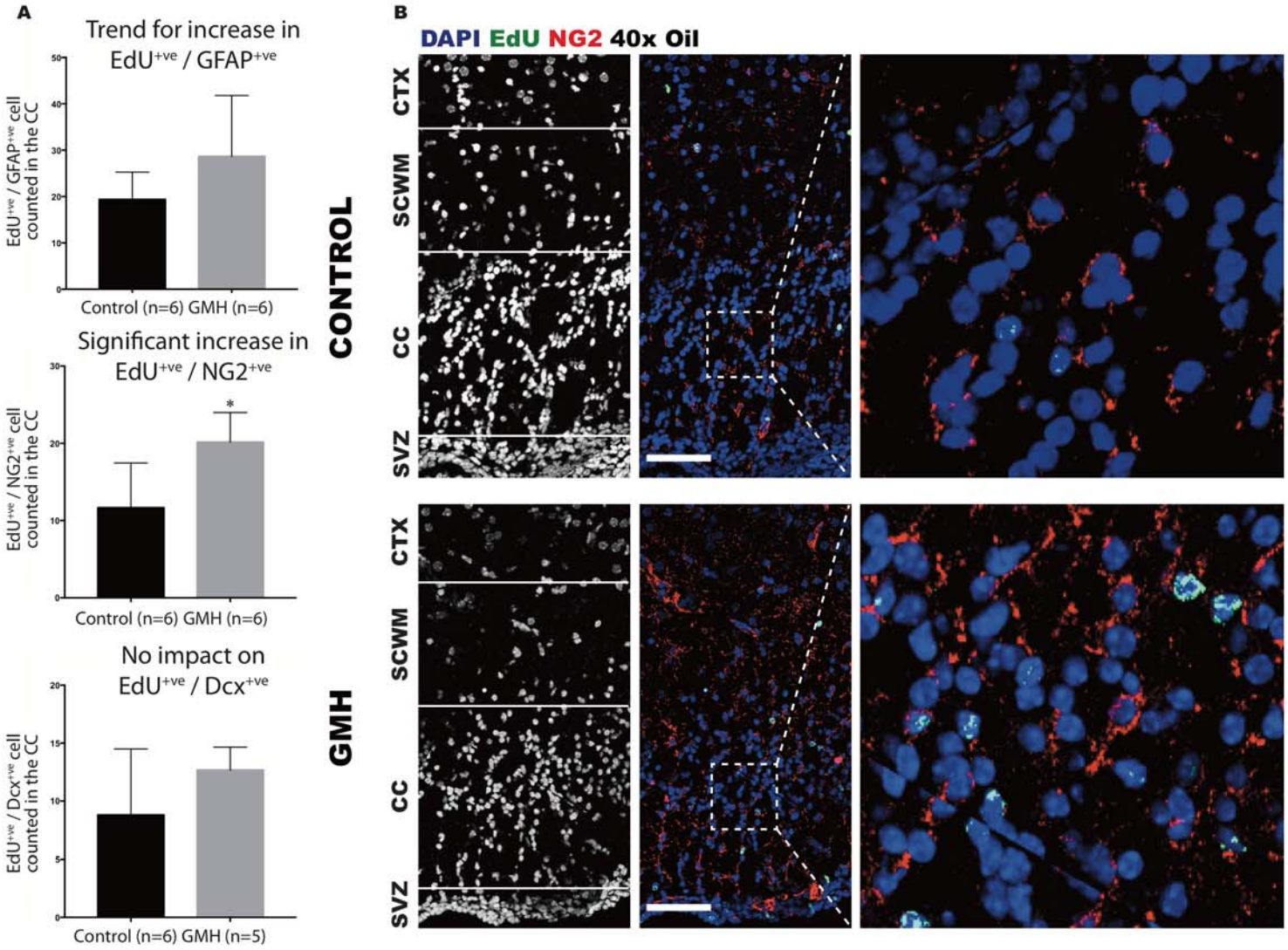
A
Trend for increase in
EdU+ve / GFAP+ve
EdU+ve / GFAP+ve cell counted in the CC
Control (n=6) GMH (n=6)
Significant increase in
EdU+ve / NG2+ve
EdU+ve / NG2+ve cell counted in the CC
*
Control (n=6) GMH (n=6)
No impact on
EdU+ve / Dcx+ve
EdU+ve / Dcx+ve cell counted in the CC
Control (n=6) GMH (n=5)
CONTROL
GMH
B
DAPI EdU NG2 40x Oil
CTX
SCWM
CC
SVZ
CTX
SCWM
CC
SVZ

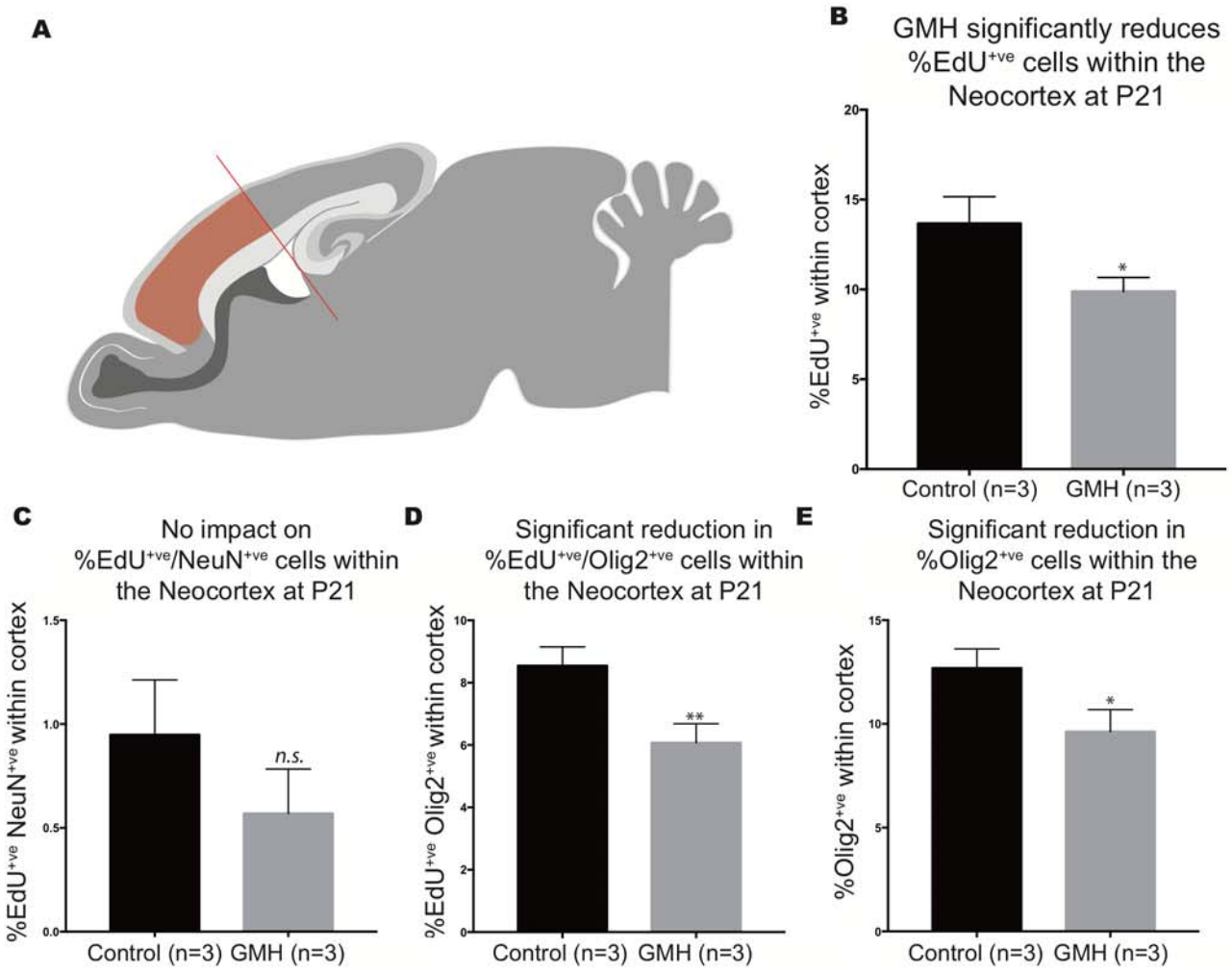
A
B
GMH significantly reduces %EdU+ve cells within the Neocortex at P21
%EdU+ve within cortex
20
15
10
5
0
*
Control (n=3)
GMH (n=3)
C
No impact on %EdU+ve/NeuN+ve cells within the Neocortex at P21
%EdU+ve NeuN+ve within cortex
1.5
1.0
0.5
0.0
n.s.
Control (n=3)
GMH (n=3)
D
Significant reduction in %EdU+ve/Olig2+ve cells within the Neocortex at P21
%EdU+ve Olig2+ve within cortex
10
8
6
4
2
0
**
Control (n=3)
GMH (n=3)
E
Significant reduction in %Olig2+ve cells within the Neocortex at P21
%Olig2+ve within cortex
15
10
5
0
*
Control (n=3)
GMH (n=3)

A

Gene	Fold Change	P-value	Gene	Fold Change	P-value
Ccne1	-2.68592	0.036546	Notch2	-26.1515	0.012798
Cxcl12	-4.95	0.032467	Sox2	-8.14351	0.020801
Ep300	-13.4554	0.039858	Tubb3	-3.08647	0.00427
Kat2a	-8.75718	0.037189	Hsp90ab1	1.965691	0.034359

B

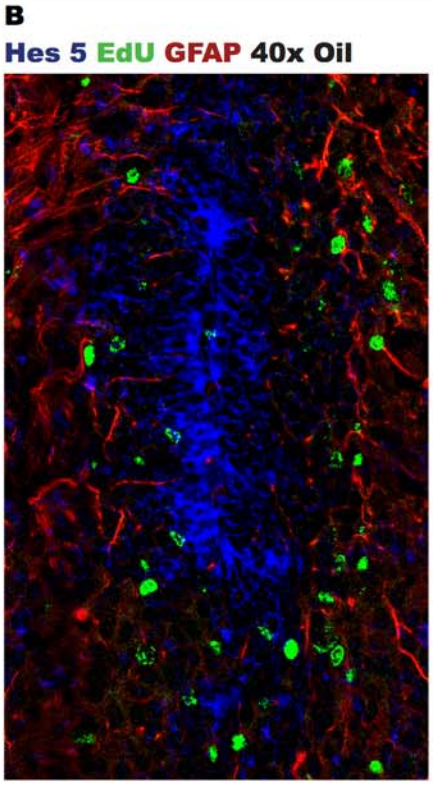

C

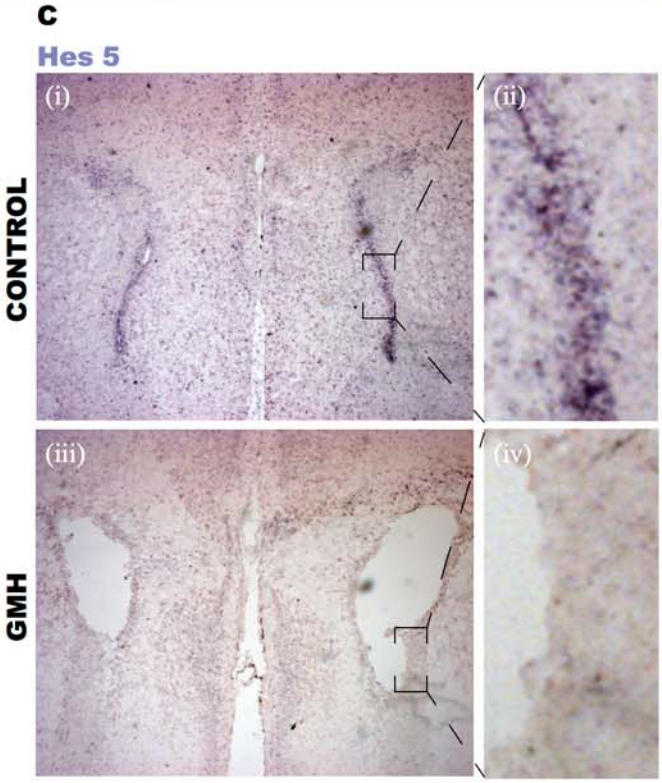

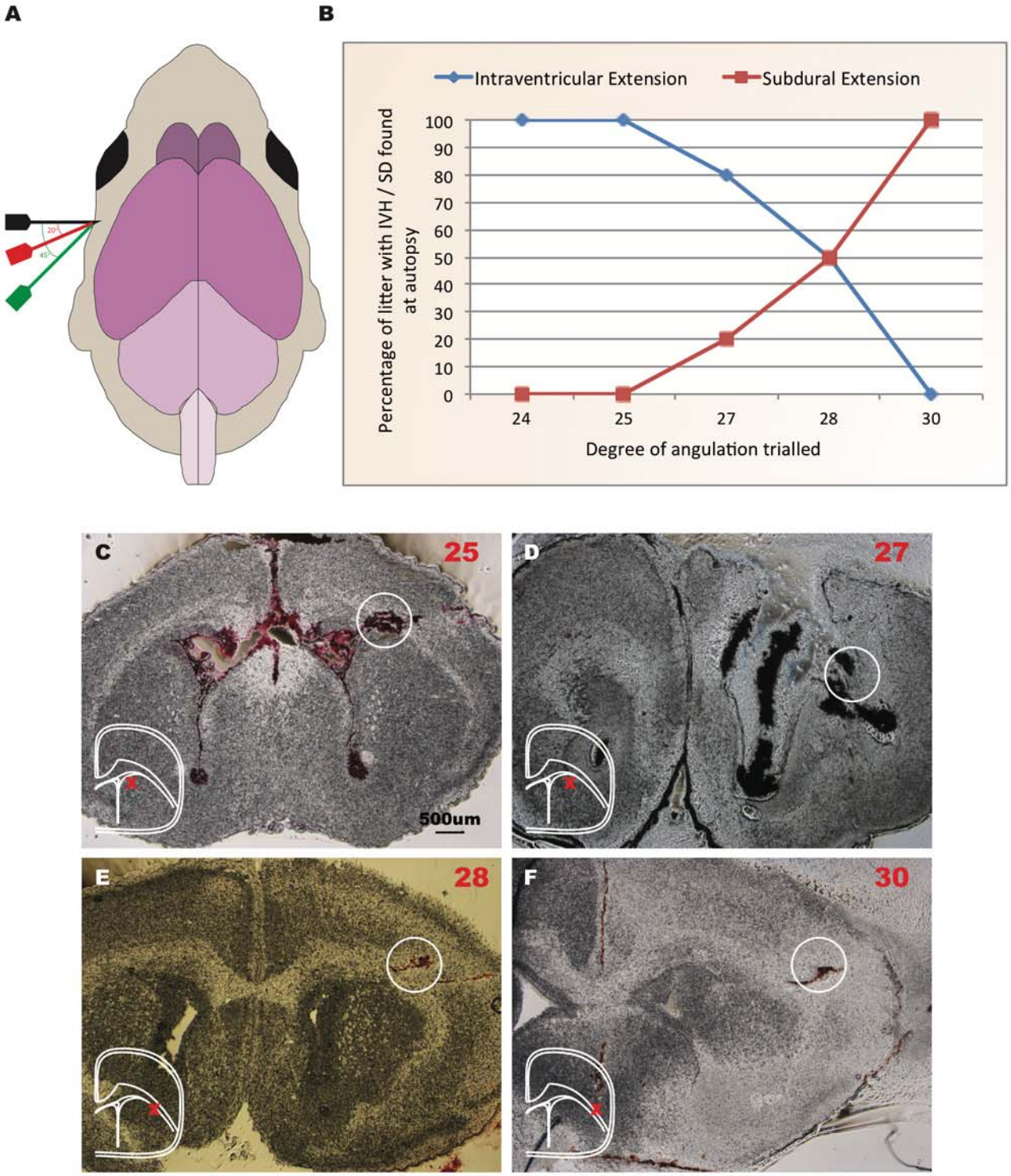
A
B
Intraventricular Extension
Subdural Extension
Percentage of litter with IVH / SD found at autopsy
100
90
80
70
60
50
40
30
20
10
0
24
25
27
28
30
Degree of angulation trialled
C
25
500um
D
27
E
28
F
30

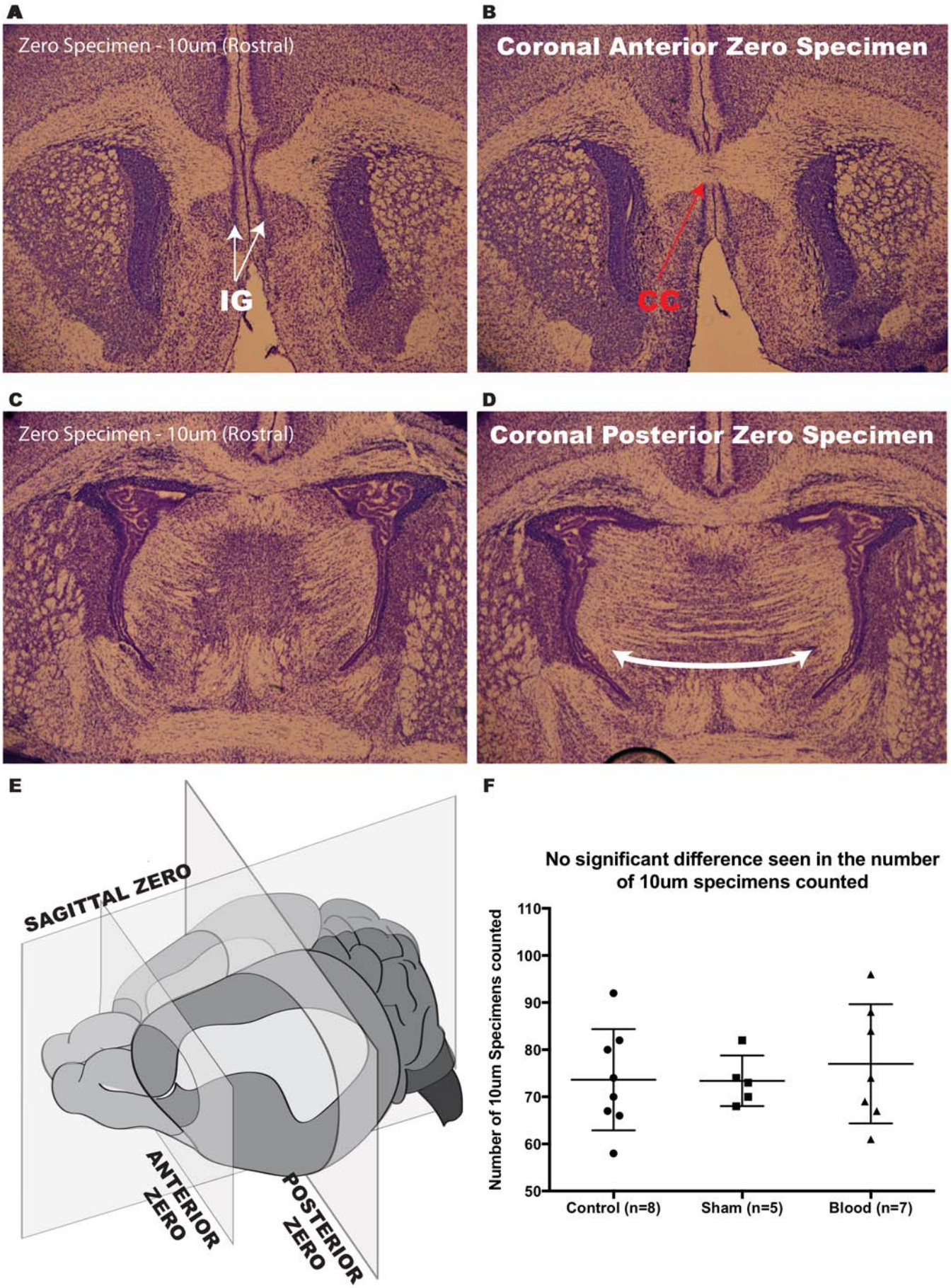
A
Zero Specimen - 10um (Rostral)
IG
B
Coronal Anterior Zero Specimen
CC
C
Zero Specimen - 10um (Rostral)
D
Coronal Posterior Zero Specimen
E
SAGITTAL ZERO
ANTERIOR ZERO
POSTERIOR ZERO
F
No significant difference seen in the number of 10um specimens counted
Number of 10um Specimens counted
110
100
90
80
70
60
50
Control (n=8)
Sham (n=5)
Blood (n=7)

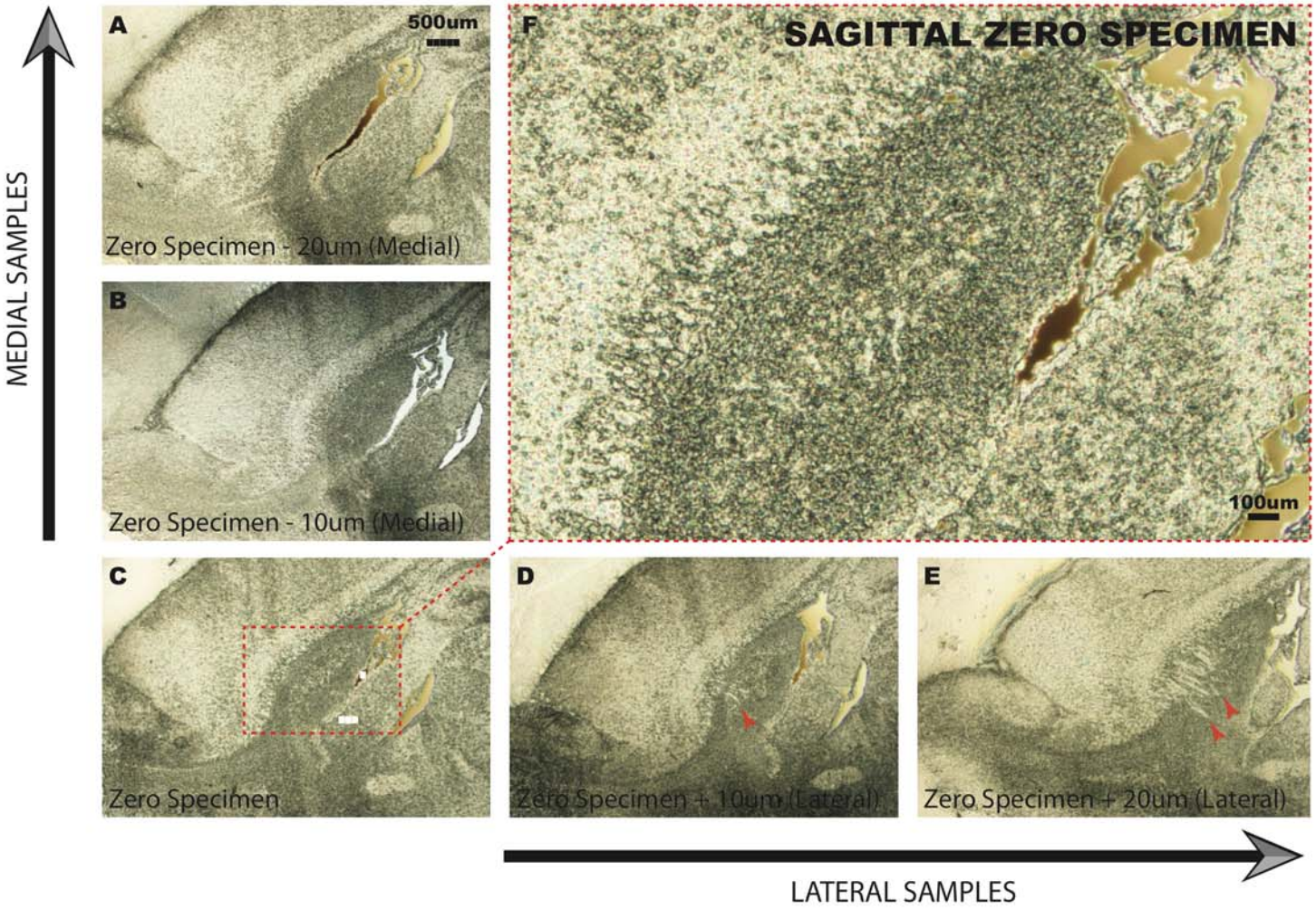
A
500um
Zero Specimen - 20um (Medial)
B
Zero Specimen - 10um (Medial)
C
Zero Specimen
F
SAGITTAL ZERO SPECIMEN
100um
D
Zero Specimen + 10um (Lateral)
E
Zero Specimen + 20um (Lateral)
MEDIAL SAMPLES
LATERAL SAMPLES

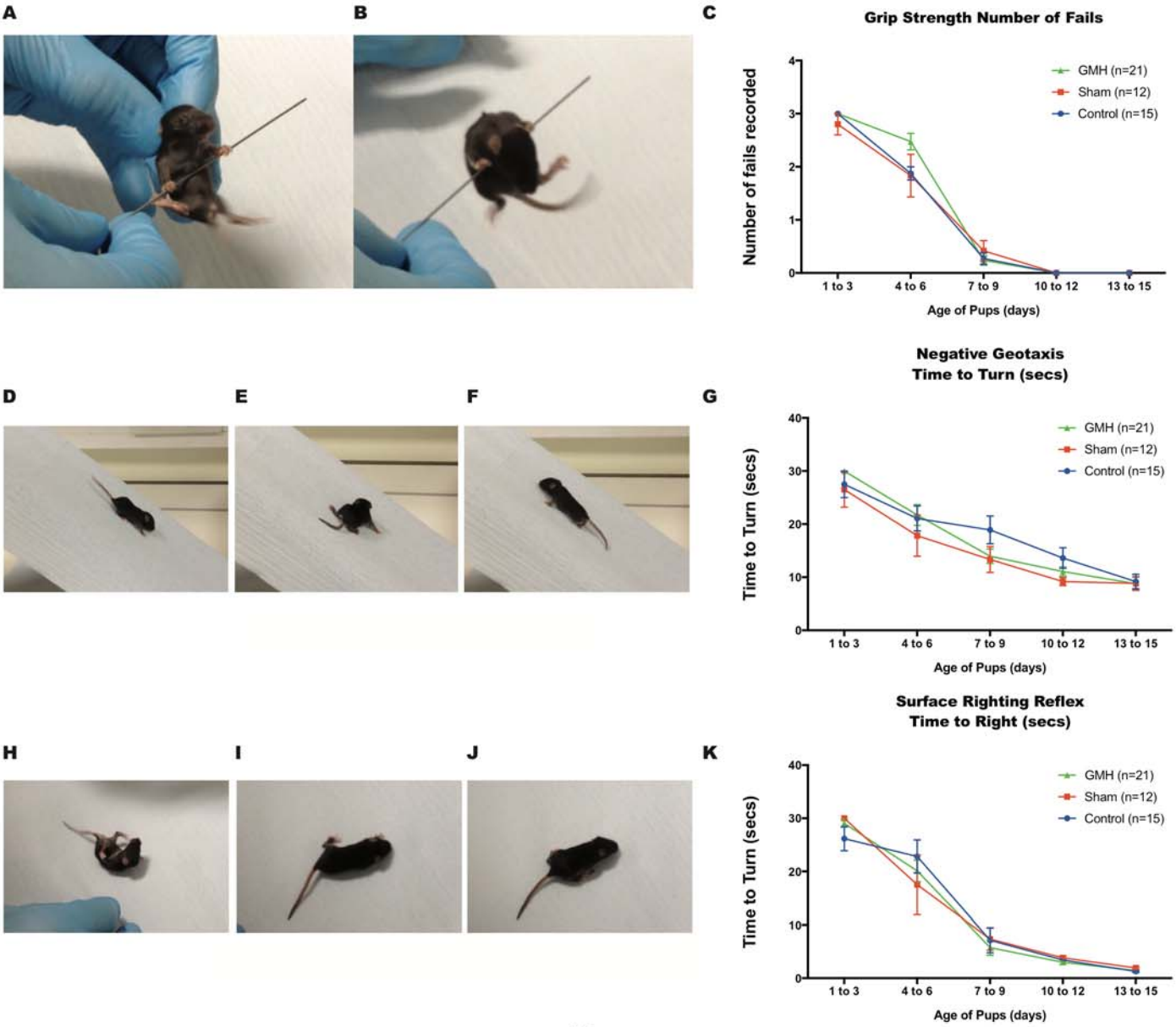
A
B
C
Grip Strength Number of Fails
Number of fails recorded
GMH (n=21)
Sham (n=12)
Control (n=15)
1 to 3
4 to 6
7 to 9
10 to 12
13 to 15
Age of Pups (days)
D
E
F
G
Negative Geotaxis
Time to Turn (secs)
Time to Turn (secs)
H
I
J
K
Surface Righting Reflex
Time to Right (secs)

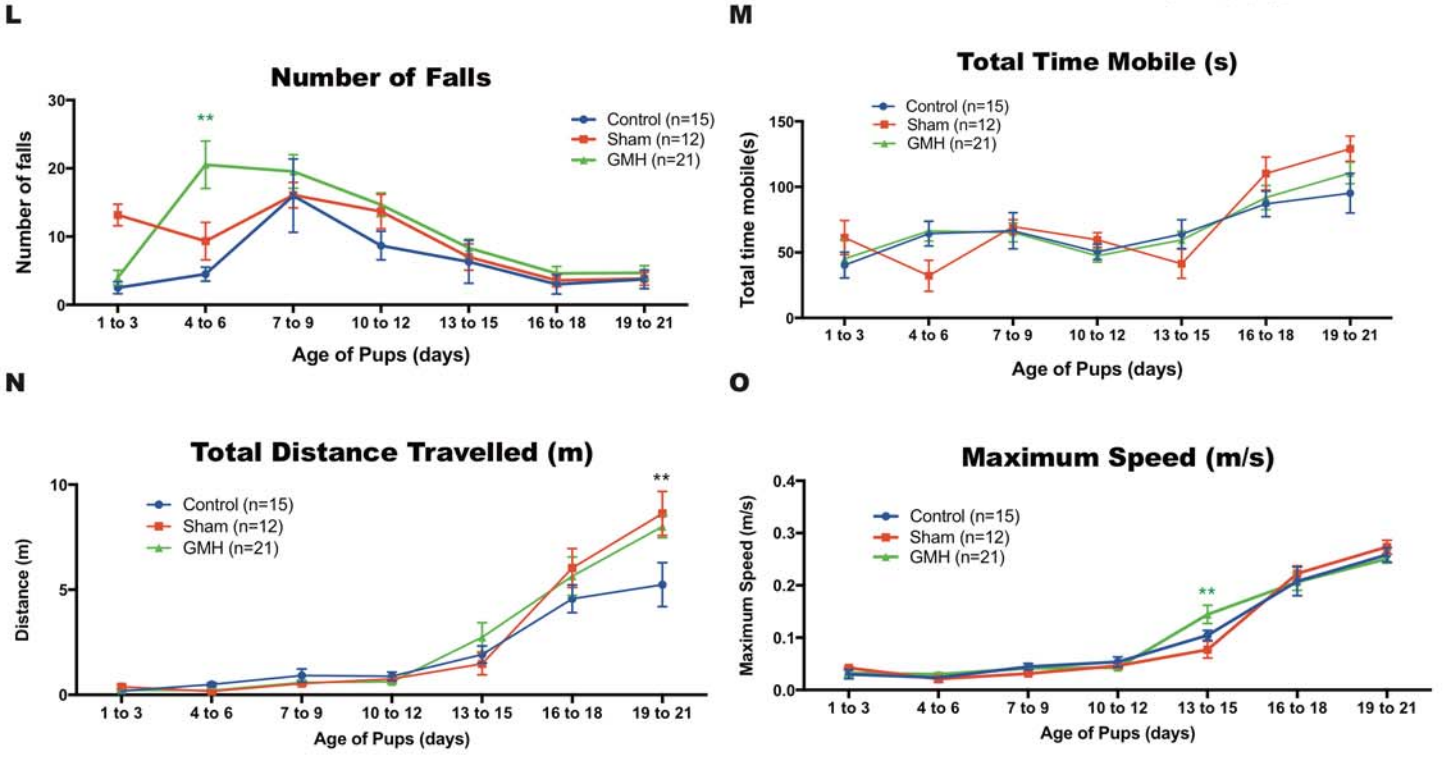
L
Number of Falls
Number of falls
Control (n=15)
Sham (n=12)
GMH (n=21)
**
1 to 3
4 to 6
7 to 9
10 to 12
13 to 15
16 to 18
19 to 21
Age of Pups (days)
M
Total Time Mobile (s)
Total time mobile(s)

N
Total Distance Travelled (m)
Distance (m)
O
Maximum Speed (m/s)
Maximum Speed (m/s)

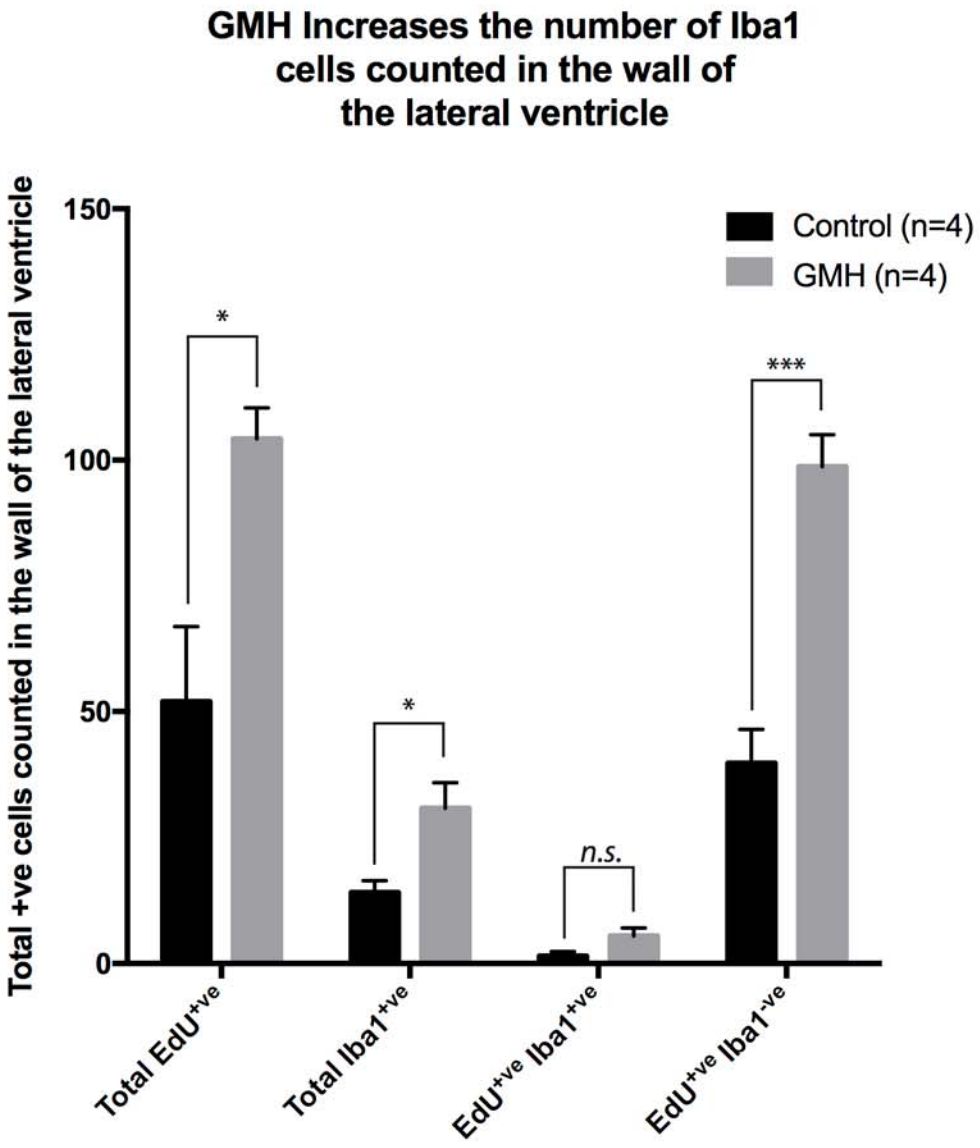
GMH Increases the number of Iba1 cells counted in the wall of the lateral ventricle
Total +ve cells counted in the wall of the lateral ventricle
150
100
50
0
Control (n=4)
GMH (n=4)
*
*
n.s.
***
Total EdU+ve
Total Iba1+ve
EdU+ve Iba1+ve
EdU+ve Iba1-ve